Conductivity and Hall effect in the two-dimensional Hubbard model

Puru Voruganti, Andrey Golubentsev, and Sajeev John
Department of Physics, University of Toronto, Toronto, Ontario, Canada M5S 1A7
(Received 5 September 1991; revised manuscript received 27 January 1992)

A path-integral field-theoretic derivation of electromagnetic linear response for the two-dimensional Hubbard model is given. We find, remarkably, that changes in the Fermi-surface topology associated with incommensurate planar spin-density-wave saddle points induce a change in sign of the Hall coefficient at dopings $\delta_H = 0.02$–0.5 for $U/t = 2$–10. The change in sign is not affected by short-range magnetic domains. We delineate from first principles an anomalous temperature dependence of the Hall carrier density at dopings close to δ_H. An additional anisotropic component to the usual dc conductivity is nonvanishing for certain types of spirals. The paper extends the Bloch-Boltzmann theory to the case of untraditional Fermi liquids where the damping of the quasiparticles is $\Gamma(\epsilon) \sim \max(k_B T, \epsilon)$.

The connection of the two-dimensional Hubbard model with high-temperature superconductivity[1] has sparked broad interest in the nature of Mott insulators.[2] Two-dimensional (2D) Mott-Hubbard insulators exhibit unconventional electronic, optical, and magnetic behavior when doped with mobile charge carriers. Various approximations including the random-phase approximation (RPA),[3] t-matrix methods,[4] and Monte Carlo techniques[5] have been used. One specific aim of these studies is to show that even in the presence of weak interlayer couplings, the Hubbard model may give rise to a nontraditional Fermi liquid,[6] where the excitations near the Fermi surface are no longer sharp but rather have vanishing spectral weight and damping proportional to the temperature and not temperature squared. This is borne out by inverse photoemission,[7] optical-conductivity studies,[8] neutron scattering,[9] as well as low-energy transport measurements. Transport measurements like resistivity[10] and Hall number[11,12] on high-quality single crystals and films further establish the anomalous properties of the normal state of the copper-oxide systems. Whether these features are related to a ground state that can be approximated by mean-field theory[13,14] or are essentially nonperturbative effects involving topological defects in the magnetic order remains to be established. It is our aim in this paper to identify anomalies in transport and electromagnetic response that may be attributed to conventional mean-field effects and isolate them from other anomalies which may require the incorporation of strong fluctuations or other unconventional effects. We find that certain anomalies in the Hall data arise from mean-field effects whereas these same effects alone are incapable of explaining the marginal-Fermi-liquid response observed in the Mott-insulator to Fermi-liquid crossover regime deduced from the resistivity data.

At half-filling, mean-field theory is extremely satisfactory in delineating the properties of the antiferromagnetic state where fluctuation corrections can be obtained in a $1/S$ expansion with S the on-site magnetization. In some recent papers,[15,16] we have discussed using analytical methods the mean-field and fluctuation magnetic and electronic properties of these systems, starting from the microscopic one-band Hubbard model at arbitrary filling. One important result of this analysis at the mean-field level was the closure of the Mott-Hubbard semiconductor gap with doping and the concomitant crossover to Fermi-liquid behavior at dopings slightly greater than that required for superconductivity. At the fluctuation level, we demonstrated from first principles that the doping-induced twist of the magnetic mean field gives rise to strong spin-charge coupling and that intraband electronic excitations in the Mott phase may be described as a charge-plus-spin-twist collective mode. In addition, interband electronic excitations occur across an indirect semiconductor gap for small doping. The spectrum of low-energy collective spin fluctuations exhibits three Goldstone modes, all of which have a crystal momentum corresponding to the momentum separation between the top of the lower Mott-Hubbard band and the bottom of the upper Mott-Hubbard band. This makes the indirect interband gap accessible to spin-wave-assisted optical transitions. In this paper, we extend our discussion of doped Mott insulators to include coupling to an external electromagnetic field. We also generalize our previous mean-field studies to finite temperature. We find that the Hall coefficient is positive at very small doping for an incommensurate spiral magnetic state but that the curvature of the Fermi surface changes greatly with further doping leading to a change in sign for this response coefficient at a critical density δ_H. In the vicinity of δ_H, the Hall density n_H is very sensitive to temperature. This work is in contrast to other explanations of these transport effects which invoke either extensions of the Hubbard Model involving additional bands or higher-order terms in hopping.[17] However, mean-field theory gives no plausible microscopic account for the linear temperature dependence of the ordinary resistivity.

Fluctuation effects as well as other interactions may be required for an understanding of this aspect of the non-Fermi-liquid behavior of the nonsuperconducting metallic phase of these compounds.

Fluctuation effects also give rise to quantitative modifications of the relevant temperature and energy scales governing the phase diagrams and transport anomalies which we have described at the mean-field level. At a very high temperature T_M, the mean-field theory predicts a transition from the antiferromagnetic insulator to a paramagnetic metal in which the static local moment and the associated gap between the Mott-Hubbard bands vanish. This is to be distinguished from the antiferromagnetic insulator to paramagnetic insulator transition which occurs at the Nèel temperature $T_N \ll T_M$. The Nèel temperature is sensitive to spin-wave and other fluctuation effects which conspire to destroy the three-dimensional long-range ordering but preserve the Mott-Hubbard gap. The ensuing paramagnetic insulator exhibits strong two-dimensional domain ordering well above T_N. It is likely that transport anomalies which are associated with slow *intraband* processes are affected by spin-wave renormalization effects and that the temperature scale on which they are observed experimentally is likewise reduced from our mean-field estimate. This is especially true of the thermally driven sign change and anomalous temperature dependence of the Hall coefficient. *Interband* processes which occur at time scales short compared to that of spin-wave fluctuations are less affected by corrections to mean-field theory. We anticipate, therefore that the overall electronic band structure which we obtain at mean-field level remains intact even in the absence of true long-range magnetic order, except perhaps in the high-doping regime where the energy scales of electronic and magnetic excitations become comparable.

Transport coefficients in the presence of symmetry-breaking order parameters necessarily require a microscopic treatment where the coherence factors that relate the new bands to the fundamental electrons play an important role in response functions. We extend the use of the path integrals to study the linear response to electromagnetic perturbations around nontrivial saddle points. We first derive the Bloch-Boltzman transport formulas for transport in the case of the tight-binding model and then extend the theory for the case of a magnetic background. Our discussion of transport in the Mott-Hubbard system is restricted to the study of band-structure effects arising from nontrivial magnetic ordering. We omit vertex corrections to the electromagnetic coupling which arise mainly from spin-wave corrections of order $1/S$. An incorporation of these effects leads to the replacement of the quasiparticle lifetime τ by the transport relaxation time $\tau_{\rm tr}$ in conductivity[18,19] as in the many-impurity problem.

I. LINEAR RESPONSE FOR NARROW-BAND METAL

In this section we obtain the usual conductivity and the Hall conductivity at any temperature for the case of a tight-binding Hamiltonian. This provides the necessary background for the analysis of conductivity for magnetic ground states covered in Sec. III.

A. Formalism

Without any loss of generality, we consider the narrow-band Hamiltonian

$$H = \sum_{\langle ij\rangle,\sigma} t_{ij} c^{\dagger}_{i\sigma} c_{i\sigma}, \tag{1.1}$$

where the sum $\langle ij\rangle$ denotes pairs of sites, e.g., nearest neighbors, and σ is the spin index and t_{ij} the hopping matrix elements. This model is symmetric in spin and for simplicity we suppress this index in this section and it can be accounted for by multiplying the transport coefficients by two. The electromagnetic field $\mathbf{A}$ is introduced in a gauge-invariant way[20] by replacing t_{ij} with

$$t_{ij} \rightarrow t_{ij}(A) = t_{ij} \exp\left(\frac{ie}{\hbar}\int_i^j \mathbf{A}(r)\cdot d\mathbf{r}\right). \tag{1.2}$$

The conserved current is given by functional derivative $\mathbf{J} = -\delta H/\delta \mathbf{A}$. Linear response at any temperature can be obtained from the grand canonical partition function given by

$$Z[A] = \mathrm{Tr}\{\exp[-\beta(H-\mu N)]\}, \tag{1.3}$$

where μ is the chemical potential, β the inverse temperature, and $N = \sum_i c^{\dagger}_i c_i$. In path-integral form, this can be written

$$Z[A] \equiv e^{-\beta\Omega(A)} = \mathcal{N}\int D[c^*, c]\exp\left\{-\int_0^{\beta} d\tau\, \mathcal{L}\right\}, \tag{1.4}$$

$$\mathcal{L} = c^*_i[(\partial/\partial\tau - \mu)\delta_{ij} + t_{ij}(A)]c_i,$$

with the summation over sites implied and $\mathcal{N}$ the overall normalization constant. Since the $\mathbf{A}(r)$ field is not quantized, the path-integral form gives it only τ dependence without introducing τ derivatives.[21] We approximate the continuum phase factor in $t_{ij}(A)$ so that the Hamiltonian depends only on the lattice sites $\mathbf{r}_i$,

$$\int_i^j \mathbf{A}(r)\cdot d\mathbf{r} \sim \mathbf{A}(R_{ij})\cdot \mathbf{r}_{ij}, \tag{1.5}$$

where $\mathbf{r}_{ij} = \mathbf{r}_j - \mathbf{r}_i$ and $\mathbf{R}_{ij} = (\mathbf{r}_j + \mathbf{r}_j)/2$.

The Fourier transforms for the Grassmann variables and the gauge field for the lattice with L sites are given by

$$c_j(\tau) = (1/\sqrt{\beta L})\sum_p \exp(i\mathbf{p}\cdot\mathbf{r}_j - iw_m\tau)c_p,$$

$$\mathbf{A}_{ij}(\tau) = \sum_q \exp(i\mathbf{q}\cdot\mathbf{R}_{ij} - iw_n\tau)\mathbf{A}_q, \tag{1.6}$$

where the Matsubara frequencies for the fermions is

$w_m = \pi(2m+1)/\beta$ and $w_n = 2n\pi/\beta$ for the gauge field. We have used the relativistic notation for the momentum and frequency indices, e.g., $p \equiv (\mathbf{p}, w_m)$. The electronic dispersion is given by

$$\epsilon_p = \sum_{(ij)} t_{ij} \exp(i\mathbf{p}\cdot\mathbf{r}_{ij}). \tag{1.7}$$

For the nearest-neighbor model, the dispersion becomes $\epsilon_p = -2t(\cos p_x + \cos p_y)$ where the lattice constant a_0 has been set to unity. From here on we set $\hbar = 1$. The partition function can be written $Z[A] = \mathcal{N}\int D[c^*, c]\exp(-S)$, and we find that the term of order n in $\mathbf{A}$ in the action S is given by the moment of ϵ_p with respect of $\mathbf{r}_{ij}$, or

$$[(ie)^n/n!]\int_0^\beta d\tau \sum_{\langle ij\rangle} t_{ij} c_i^*(\mathbf{A}_{ij}\cdot\mathbf{r}_{ij})^n c_j = (e^n/n!)\sum_{p,q,q_a} c_p^* \epsilon^{\delta_1\cdots\delta_n}_{p/2+q/2} c_q (A^{\delta_1}_{q_1}\cdots A^{\delta_n}_{q_n}), \tag{1.8}$$

where the upper indices on the dispersion imply differentiation, i.e., $\epsilon_p^\alpha \equiv \partial\epsilon_p/\partial p^\alpha$. The four-momenta in the sum are constrained to $\sum_{a=1,\ldots,n} q_a = p - q$. The action to quadratic order can be brought to the form

$$\begin{aligned} S &= \sum_{p,q} c_p^*(K_{pq} + V_{pq}[A])c_q, \\ V_{pq}[A] &= e\epsilon^\alpha_{p/2+q/2}A^\alpha_{p-q} \\ &\quad + (e^2/2)\epsilon^{\alpha\beta}_{p/2+q/2}\sum_k A^\alpha_{p-q-k}A^\beta_k + \ldots, \\ K_{pq} &= \delta_{pq}G_p^{-1} = \delta_{pq}(-iw_m + \epsilon_p - \mu). \end{aligned} \tag{1.9}$$

We refer to the vertex with n photons as vertex V^n.

Since transport involves absorption of energy from external sources, we must introduce a damping rate for the quasiparticles in order to obtain finite conductivities. For simplicity, we assume an isotropic damping rate for the phenomenological Green's function

$$G_p^{-1} = -iw_m + \epsilon_p - \mu + i\,\mathrm{sgn}(w_m)\Gamma. \tag{1.10}$$

The quasiparticle lifetime τ is then given by $\Gamma = 1/2\tau$. In the tradition Fermi-liquid regime,[22] one sets $\Gamma \sim (k_BT)^2/E_F \ll 1$, where E_F is the Fermi energy. An analysis of the optical data[8] for the high-T_c materials reveals instead $\Gamma(w) \propto \max(k_BT, |w|)$. In either case, transport quantities will depend only on τ since we omit vertex corrections to the electromagnetic coupling.

The Grassmann integrals over the fermionic degrees of freedom can be readily performed[21,23] using the identity $\int D\psi^\dagger D\psi \exp[\psi^\dagger(K+V)\psi] = \mathrm{Det}[K+V]$ which gives for the effective action

$$-\beta\Omega[A] = \mathrm{Tr}\ln K + \mathrm{Tr}\ln(1 + K^{-1}V[A]) \tag{1.11}$$

up to various c-number terms arising from the normalization of $Z[A]$. The particle constraint[15] for doping δ is $\langle N\rangle = -\partial\Omega/\partial\mu = L(1-\delta)$ which for weak perturbations $\mathbf{A}$ becomes

$$\langle N\rangle = (1/\beta)\sum_p G_p = \sum_{\mathbf{p}} f(\epsilon_p - \mu), \tag{1.12}$$

where f is the Fermi function $f(x) = 1/[\exp(x)+1]$ and the Matsubara sum was performed using standard techniques.[24] The first term in the effective action only plays a role in determining the Fermi energy μ and plays no role in determining the current response.

We can express the current response in terms of a spatially uniform electric component $\mathbf{a}^E_{w_n}$ and a static magnetic component $\mathbf{a}^B_{\mathbf{k}}$ via

$$\mathcal{J}_q^\alpha = -(1/V)\delta\Omega[A]/\delta A^\alpha_{-q}\big|_{\mathbf{A}=\mathbf{a}^E+\mathbf{a}^B}. \tag{1.13}$$

Here, we have defined the induced current with respect to the normalization volume V. The second term in the effective action $\Omega[A]$ in Eq. (1.11) determines the current response using the identity

$$\mathrm{Tr}\ln(1 + K^{-1}V[A]) = -\sum_{m=1}^{\infty}\mathrm{Tr}(K^{-1}V[A])^m/m. \tag{1.14}$$

Applying the definition of the current in Eq. (1.13), the current to zeroth order in the external fields is

$$\begin{aligned} \delta_0\mathcal{J}_q^\alpha &= \delta_{w_n,0}\delta_{\mathbf{q},0}(e/\beta V)\sum_p G_p\epsilon_p^\alpha \\ &= (e/V)\delta_{w_n,0}\delta_{\mathbf{q},0}\sum_{\mathbf{p}}\epsilon_p^\alpha f(\epsilon_p - \mu). \end{aligned} \tag{1.15}$$

The right-hand side (rhs) is just the paramagnetic current in the absence of any external fields and for any dispersion having inversion symmetry $\epsilon_{-p} = \epsilon_p$ this term vanishes, i.e., $\delta_0\mathcal{J}_q^\alpha = 0$.

B. Ordinary conductivity

Contributions to $\mathcal{J}_q^\alpha$ to linear order in $\mathbf{a}^E$ come from loops with two V^1 vertices and one V^2 vertex. Adding these contributions, we find

$$\delta_1^E\mathcal{J}_n^\alpha = -(e^2/V)a_n^{E\beta}\Big\{\sum_{\mathbf{p}}\epsilon_p^\alpha\epsilon_p^\beta(1/\beta)\sum_m G_{\mathbf{p},m}G_{\mathbf{p},m+n} - \sum_{\mathbf{p}}\epsilon_p^{\alpha\beta}(1/\beta)\sum_m G_{\mathbf{p},m}\Big\}, \tag{1.16}$$

where the subscripts $n, m \equiv iw_n, iw_m$. The cancellation of the $w_n = 0$ part of the rhs is necessary for finite conductivity and a consequence of gauge invariance.[25] To demonstrate the cancellation, we first define

$$\Pi(\mathbf{p}, w_n) = (1/\beta)\sum_m G_{\mathbf{p},m}G_{\mathbf{p},m+n}. \tag{1.17}$$

The second term on the rhs is independent of n and the leading contribution from the first graph can be written $\Pi(\mathbf{p}, 0) = -\partial f/\partial\epsilon_p$. Further, since $\epsilon_p^\beta\partial f/\partial\epsilon_p = \partial f/\partial p^\beta$,

we can integrate by parts in the first integral using periodic boundary conditions, and find that the $w_n = 0$ contribution of the first integral cancels the entire second term.

The imaginary-time response functions can be used to calculate the real-time retarded response at any temperature by performing the analytic continuation from the upper half-plane where $\mathrm{sgn}(w_n) > 0$ to the real axis,[24] i.e., $iw_n \to w$. This continuation must be performed, however, only after we defined the Matsubara sum as a contour integral in the complex-frequency plane. In real time, we have $\mathbf{E}_w = iw\mathbf{a}_w^E$, and therefore if we write the response to the electric field as $\delta_1^E \mathcal{J}_w^\alpha = \sigma^{\alpha\beta}(w)E^\beta$, we find the conductivity to be given by

$$\sigma^{\alpha\beta}(w) = -(e^2/V)\sum_{\mathbf{p}} \epsilon_p^\alpha \epsilon_p^\beta (1/iw)\Pi(\mathbf{p}, w), \quad (1.18)$$

where $\Pi(\mathbf{p}, w) = \Pi(\mathbf{p}, w_n)\big|_{w_n \to w}$. For processes involving absorption, we are interested in the real part of the conductivity or the imaginary part of $\Pi(\mathbf{p}, w_n)$. We evaluate $\Pi(\mathbf{p}, w)$ by introducing the advanced and retarded Green's functions[18] defined by $G_p^{R(A)} = 1/(-iw_m + \epsilon_p - \mu \pm i\Gamma)$, which are analytic in the upper and lower half-planes, respectively. Using standard techniques[18] to evaluate the Matsubara sum of the product of two Green's functions, we obtain for $I(w) = \mathrm{Im}\Pi(\mathbf{p}, w)/w$,

$$I_0 = -\int_{-\infty}^{\infty} (d\epsilon/\pi)\ \partial f/\partial\epsilon\ \Gamma^2(\epsilon)/[(\epsilon - \epsilon_p + \mu)^2 + \Gamma^2(\epsilon)]^2 \quad (1.19)$$

in the zero-frequency limit where $I_0 \equiv I(w \to 0)$. For Fermi liquids with quasiparticle damping $\Gamma \to 0$, we can approximate $\lim_{\Gamma\to 0} \Gamma^2/[x^2 + \Gamma^2]^2 = 2\pi\delta(x)/\Gamma$ giving for the dc conductivity the Bloch-Boltzman formula

$$\sigma_0^{\alpha\beta} \equiv (e^2\tau/V)\sum_{\mathbf{p}} \epsilon_p^\alpha \epsilon_p^\beta (-\partial f/\partial\epsilon_p), \quad (1.20)$$

where $\sigma_0^{\alpha\beta} \equiv \mathrm{Re}\sigma^{\alpha\beta}(w \to 0)$. Integrating by parts, we find the rhs is proportional to $e^2 \int d^2p\, \epsilon_p^{\alpha\beta} f(\epsilon_p - \mu)$. For parabolic dispersions, the dc conductivity is given by the Drude formula $\sigma_0 = e^2\tau n/m$, where $n = \langle N\rangle/V$. However, in the nonparabolic case where the second derivative of the dispersion is nontrivial, we find that the conductivity acquires a temperature dependence from the bandwidth W of order T/W beyond the temperature effects arising from τ.

In the presence of strong correlations, the narrow-band system has an additional complication that Γ is not necessarily small compared to the Fermi energy. In fact, in the normal state of the copper-oxide superconductors, one finds $\Gamma(\epsilon) \sim \alpha\ \max(k_BT, \epsilon)$ (Refs. 8 and 9) with α ranging from 1 to 10. In this case, the appropriate zero-temperature formula is instead the full formula given in Eq. (1.19). We plot the function $I_\alpha = \alpha I_0/\beta^2$ for various values of α in Fig. 1. There is a significant deviation of I_α from the conventional answer $I_\alpha = (1/2\beta)(-\partial f/\partial\epsilon_p)$ for quasiparticles near the Fermi surface when $\alpha = 1, 2$. The exact integral cannot be performed analytically, but

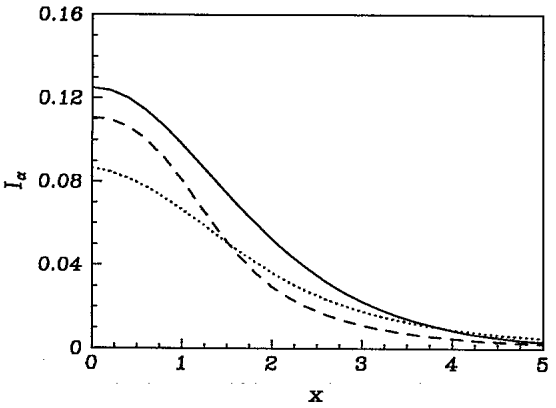

FIG. 1. An exact evaluation of the Matsubara sum I_α vs $x = (\epsilon_p - \mu)/k_BT$ with $\Gamma = \alpha\ \max(k_BT, \epsilon)$ at $\alpha = 1, 2$, shown as dashed and dotted lines, respectively. The conventional result is shown as a solid line.

we may still write $I_0 = \tau(-\partial g/\partial\epsilon_p)$, where $g(\epsilon) = f(\epsilon)$ for $\alpha << 1$. This implies that when Γ is sufficiently large, the Drude formula is replaced $\sigma_0 = e^2\tau n^*(T)/m$, where $n^*(T) = (1/V)\int d^2p\ g(\epsilon_p)$. Since $\mu(T)$ is fixed by the particle constraint, the integral over $g(\epsilon_p)$ must be temperature dependent. Therefore, residual temperature dependences can arise in the usual conductivity for very narrow bands from two independent sources, nonparabolic effects which are of order T/W and short quasiparticle lifetimes effects proportional to $\alpha(T/W)$. It is precisely when the Landau Fermi-liquid assumption of a long-lived quasiparticle is no longer valid that the Bloch-Boltzmann formula is modified as in Eq. (1.19).

C. Hall conductivity

Whereas the terms to order e^2 give the usual conductivity, the terms of order e^3 give rise to the Hall conductivity. The next-order terms arise from loops with three

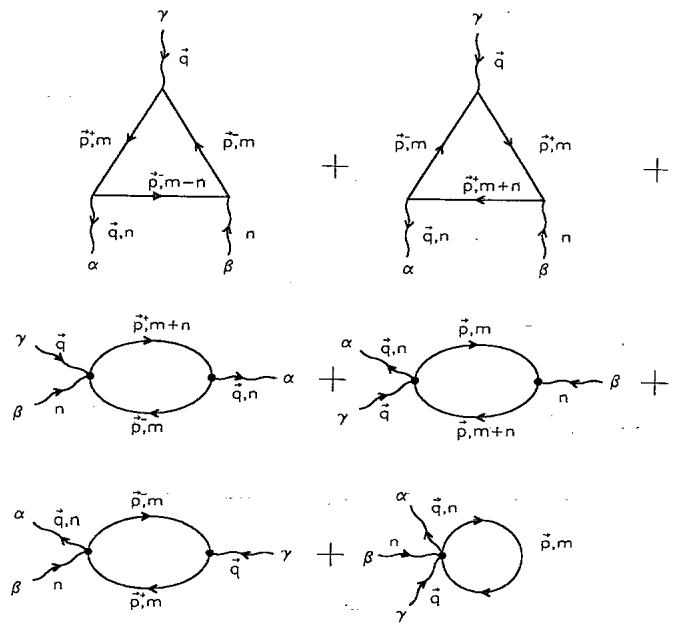

FIG. 2. The six diagrams of order e^3 in the free energy $\Omega[A]$ that contribute to the Hall conductivity.

V^1 vertices, or one V^1 and one V^2 vertex, or finally with one V^3 vertex. Furthermore, each such diagram after differentiation with respect to $\mathbf{A}$ gives terms quadratic in $\mathbf{a}^E$, quadratic in $\mathbf{a}^B$, or linear in each. The subdiagrams that lead to the Hall coefficient contain one power of $\mathbf{a}^E$ and one power of $\mathbf{a}^B$. For simplicity we confine our attention to these diagrams which are shown in Fig. 2. The induced current can be brought to the form

$$\delta_2 \mathcal{J}^{\alpha}_{q,w_n} = (e^3/V\beta) a^{E\beta}_{w_n} a^{B\gamma}_{q} \sum_{\mathbf{p}} \Big\{ \epsilon^{\alpha\beta\gamma}_{p} \sum_{m} G_{\mathbf{p},m} + \epsilon^{\alpha}_{p}\epsilon^{\gamma}_{p} \Big[\epsilon^{\beta}_{p-q/2} \sum_{m} G_{p^-,m} G_{p^+,m} G_{p^-,m-n} + \epsilon^{\beta}_{p+q/2} \sum_{m} G_{p^-,m} G_{p^+,m} G_{p^+,m+n} \Big] - \epsilon^{\alpha}_{p}\epsilon^{\beta\gamma}_{p} \sum_{m} G_{p^-,m} G_{p^+,m+n} - \epsilon^{\beta}_{p}\epsilon^{\alpha\gamma}_{p} \sum_{m} G_{\mathbf{p},m} G_{\mathbf{p},m+n} - \epsilon^{\gamma}_{p}\epsilon^{\alpha\beta}_{p} \sum_{m} G_{p^-,m} G_{p^+,m} \Big\}, \tag{1.21}$$

where $p^{\pm} = \mathbf{p} \pm \mathbf{q}/2$. The first term corresponds to the diagram with one V^3 vertex, the next two to the triangle diagrams, and the last three to the two-vertex graphs in Fig. 2. It is straightforward to show using the same integration by parts performed for the usual conductivity that the $q = 0$, $w_n = 0$ contributions from the first five diagrams exactly cancel the entire last diagram with one V^3 vertex. We are primarily interested in the zero-frequency, long-wavelength limit of the response. Writing $\delta_2 \mathcal{J}^{\alpha}_{q,w} = \sigma^{\alpha\beta\epsilon}_{H}(w) E^{\beta}_{w} B^{\epsilon}_{q}$, we notice that the real part of $\sigma^{\alpha\beta\epsilon}_{H}(w)$ requires us to evaluate the real part of each Matsubara sum to linear order in q and w_n. The last two-vertex graph is independent of w_n and its contribution to linear order in q vanishes since q appears symmetrically as $p^{\pm}$.

Not only do terms independent of w_n cancel but also all terms independent of $\mathbf{q}$, e.g., the second two-vertex diagram. The $\mathbf{q} = 0$ part of the triangle graphs can be brought to the form

$$(e^3/V\beta) a^{E\beta} a^{B\gamma} \sum_{\mathbf{p}} [\epsilon^{\alpha\gamma}_{p}\epsilon^{\beta}_{p} + \epsilon^{\beta\gamma}_{p}\epsilon^{\alpha}_{p}] \sum_{m} G^2_{\mathbf{p},m} G_{\mathbf{p},m+n} \tag{1.22}$$

using $G^2_p = -\partial G_p/\partial \epsilon_p$ and integrating by parts. The first term in the above equation cancels the entire second two-vertex graph. The other term cancels the $\mathbf{q} = 0$ piece of the first two-vertex graph as can be easily seen from Eq. (1.21).

It is only the first three diagrams in Fig. 2 that contribute to the Hall conductivity in the zero frequency, long-wavelength limit. We expand $\epsilon^{\beta}_{p-q/4}$ and the first three Matsubara sums using $G_{p^{\pm},m} = G_{\mathbf{p},m} \mp (q^{\delta}/2)\epsilon^{\delta}_{p} G^2_{\mathbf{p},m}$ and define the frequency sum

$$\Pi_H(\mathbf{p}, w_n) = (1/\beta) \sum_{m} G^2_{\mathbf{p},m} (G_{\mathbf{p},m+n} - G_{\mathbf{p},m-n}). \tag{1.23}$$

In terms of Π_H, the Hall response is given by

$$\delta_2 \mathcal{J}^{\alpha}_{q,w_n} = (e^3/2V)\, a^{E\beta} q^{\delta} a^{B\gamma} \times \sum_{\mathbf{p}} (\epsilon^{\beta\delta}_{p}\epsilon^{\alpha}_{p}\epsilon^{\gamma}_{p} - \epsilon^{\alpha}_{p}\epsilon^{\beta\gamma}_{p}\epsilon^{\delta}_{p}) \Pi_H(\mathbf{p}, w_n). \tag{1.24}$$

Writing $B^{\epsilon} = \varepsilon^{\epsilon\delta\gamma} i q^{\delta} a^{B\gamma}$ and exchanging γ, δ in the second term of the momentum sum, the Hall conductivity becomes

$$\sigma^{\alpha\beta\epsilon}_{H}(w) = (e^3/2V) \sum_{\mathbf{p}} \epsilon^{\alpha}_{p} \varepsilon^{\epsilon\gamma\delta} \epsilon^{\gamma}_{p} \epsilon^{\beta\delta}_{p} \Pi_H(\mathbf{p}, w)/w, \tag{1.25}$$

where as before, we must evaluate Π_H at $iw_n \to w$. After a lengthy calculation,[18] we obtain

$$I_H = \tfrac{4}{3} \int_{-\infty}^{\infty} (d\epsilon/\pi)\, (-\partial f/\partial \epsilon)\, \Gamma^3(\epsilon)/[(\epsilon - \epsilon_p + \mu)^2 + \Gamma^2(\epsilon)]^3, \tag{1.26}$$

where $I_H \equiv -\lim_{w\to 0} \mathrm{Re}\Pi_H(\mathbf{p}, w)/w$. For $\Gamma \to 0$, we may approximate $[\mathrm{Im}G^R]^3$ by $\lim_{\Gamma\to 0} \Gamma^3/[x^2 + \Gamma^2]^3 = (3\pi/8\Gamma^2)\delta(x)$. Substituting this into the previous equation and defining the Hall conductivity $\sigma^{\alpha\beta\epsilon}_{H} \equiv \sigma^{\alpha\beta\epsilon}_{H}(w \to 0)$, we arrive at

$$\sigma^{\alpha\beta\epsilon}_{H} = -(e^3\tau^2/V) \sum_{\mathbf{p}} \epsilon^{\alpha}_{p} (\boldsymbol{\epsilon}_p \times \boldsymbol{\nabla})^{\epsilon} \epsilon^{\beta}_{p}\, (-\partial f/\partial \epsilon_p), \tag{1.27}$$

which is the standard Bloch-Boltzman result for Fermi liquids. Therefore, when the bandwidth is finite, the conventional result holds in the traditional Fermi-liquid regime of small damping rates. For parabolic bands, we can partially integrate the above formula to obtain $\sigma_H \equiv \sigma^{xyz}_{H} = -e^3\tau^2 n/m^2$ at any temperature. For the nonparabolic case, the momentum sum becomes temperature dependent of order T/W. Defining the Hall coefficient $R_H = \sigma_H/\sigma^{xx}\sigma^{yy}$, $R_H^{-1} = -ne$ for parabolic bands, but it acquires a well-known temperature dependence again of order T/W for the narrow-band case.

In addition to this bandwidth effect for nonparabolic bands, we examine the implications of relaxing the assumption of small quasiparticle damping to the form $\Gamma(\epsilon) = \alpha \max(k_B T, \epsilon)$. As shown in Fig. 3, the exact integral $I^{\alpha}_H = \alpha^2 I_H/\beta^3$ from Eq. (1.26) differs significantly from the Fermi-liquid result $I^{\alpha}_H = (1/2\beta)(-\partial f/\partial \epsilon_p)$ for $\alpha = 1, 2$. The larger widths can be accounted for by writing $I_H = -2\tau^2 \partial h/\partial \epsilon_p$, where $h(\epsilon_p)$ is some new function

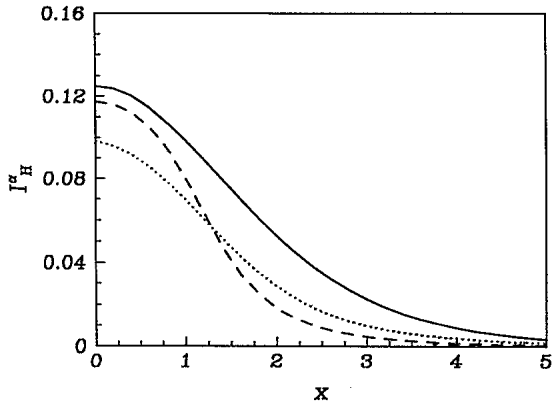

FIG. 3. An exact evaluation of the Matsubara sum I_H^α vs $x = (\epsilon_p - \mu)/k_BT$ with $\Gamma = \alpha \max(k_BT, \epsilon)$ at $\alpha = 1, 2$, shown as dashed and dotted lines, respectively. The conventional result is shown as a solid line.

and approaches $f(\epsilon_p - \mu)$ for small Γ. Importantly, this implies that even for parabolic bands, σ_H is no longer proportional to n but some temperature-dependent effective $n_H(T)$. The microscopic calculation of the Hall conductivity shows that an anomalous quasiparticle width leads to a residual temperature dependence for the Hall coefficient proportional to $\alpha(T/W)$.

In light of the dependence of the transport quantities on the subtleties of the bandwidth and Γ, a calculation of $\Gamma(\mathbf{p}, \epsilon)$ in the regime of strong correlations is important. Equally imperative are the physical scattering processes that lead τ to be replaced by $\tau_{\rm tr}$ in the interacting case. We can alternatively assume that interactions drive the narrow-band Fermi liquid into a new mean-field state which incorporates the most singular interaction channels. For example, at half-filling the 2D Hubbard model is unstable towards antiferromagnetic ordering. Likewise, at small doping a magnetic state could arise such as in spiral or incommensurate antiferromagnetism.[15,16] The quasiparticles of these states may also have a nontrivial damping, but since this is outside the scope of this article, we assume that the resulting particles have long lifetimes and therefore residual temperature dependences should arise only from the nonparabolic dispersions. We find nevertheless that the rich magnetic phase diagram itself exhibits dramatic temperature dependences for the Hall coefficient and a doping-induced sign change.

II. MAGNETIC GROUND STATES IN THE HUBBARD MODEL

The copper oxide superconductors are well approximated[1] by a nearest-neighbor tight-binding one-band Hamiltonian with a strong on-site repulsive interaction. In the presence of external electromagnetic fields, the Hubbard model is

$$H = \sum_{\langle ij\rangle,\sigma} t_{ij}(A) c_{i\sigma}^\dagger c_{j\sigma} + U \sum_i n_{i\uparrow} n_{i\downarrow}, \tag{2.1}$$

where $n_{i\sigma} = c_{i\sigma}^\dagger c_{i\sigma}$.

A. Saddle-point approximation

To evaluate the ground-state properties, we express the grand canonical partition function using functional integrals as before and obtain for the action $S = \int_0^\beta d\tau\, \mathcal{L}$, with the Lagrangian density

$$\mathcal{L} = \sum_{\langle ij\rangle} \psi_i^\dagger [(\partial_\tau - \mu_0)\delta_{ij} + t_{ij}(A)]\psi_j - (U/4) \sum_i (\psi_i^\dagger \sigma^\mu \psi_i)^2. \tag{2.2}$$

Here, we have introduced the Grassmann spinor $\psi_i = (c_{i\uparrow}, c_{i,\downarrow})$, and the matrices are defined as $\sigma^0 = I$, the identity matrix with $\sigma^a, a = 1, 2, 3$ being the three Pauli spin matrices.[23] The quartic Hubbard term can be brought to a quadratic form by using a four-component Hubbard-Stratonovich field[26] $\Phi^\mu = (\rho, \phi)$ corresponding to the charge density and the three spin components, respectively. This decomposition is particularly relevant for the Hubbard model in light of the antiferromagnetic metal-insulator transition that occurs at half-filling. The resulting partition function is

$$Z = \mathcal{N} \int D[\psi, \psi^*, \Phi^\mu] e^{-S}, \tag{2.3}$$

$$\mathcal{S} = \int_0^\beta d\tau \{ \psi_i^* [(\partial_\tau - \mu_0)\delta_{ij} + t_{ij}]\psi_j + U\Phi_i^\mu \Phi_i^\mu - U\, \Phi_i^\mu \psi_i^\dagger \sigma^\mu \psi_i \}.$$

Here, the summation over nearest neighbors, sites, and spins is implied. In addition to the Fourier transforms for the fermion and gauge fields in Eq. (1.6), we implement for the order-parameter fields the transformation

$$\Phi_i^\mu(\tau) = \sum_{k,n} \exp(i\mathbf{k}\cdot\mathbf{r}_i - iw_n\tau)\Phi_k^\mu. \tag{2.4}$$

The Gaussian fields satisfy $\Phi_k^\mu = \Phi_{-k}^{*\mu}$. The action in Fourier space requires we introduce a matrix corresponding to the Gaussian fields via $M_{pq} = \Phi_{p-q}^\mu \sigma^\mu$ and with the convention that repeated indices are summed this gives

$$S = \beta L U \Phi_p^{*\mu} \Phi_p^\mu - \psi_p^\dagger [K_{pq} + V_{pq}(A) + U M_{pq}]\psi_q. \tag{2.5}$$

Here, the spin-diagonal matrices K and V can be read off from Eq. (1.9).

In a previous paper,[16] we demonstrated a variety of self-consistent saddle points in the absence of electromagnetism. These ground states Φ_0^μ consisted of uniform charge density $\rho_0 = n$ and planar magnetic order parametrized by $\Phi_Q^- \equiv \Phi_Q^x - i\Phi_Q^y = S$ for some $\mathbf{Q}$ that was self-consistently determined as a function of U/t and δ. For any U/t, we showed that commensurate antiferromagnetism at half-filling evolves to uniform spiral states $\mathbf{Q} \neq \mathbf{Q}_0 \equiv (\pi, \pi)$ at nonzero doping. These states are plausible mean-field approximations for the normal state of the metallic and semiconducting regions of the phase diagram appropriate to the cuprates from their optical and transport properties. These re-

sults suggest that the incorporation of fluctuation effects may then lead to a complete description of their electromagnetic response. Unlike the zero-temperature phase diagram extracted before, we are interested here in the finite-temperature phase diagram to determine if a residual temperature dependence to R_H can arise from the temperature dependence of $\mathbf{Q}$ and S alone in the limit of long-lived quasiparticles.

To obtain the finite-temperature phase diagram, we must evaluate the free energy from Ω. For a general saddle point, Φ^μ can be decomposed into mean-field and fluctuation parts as $\Phi^\mu \rightarrow \Phi_0^\mu + \Phi^\mu$, $M \rightarrow M_0 + M$. The electron Green's functions in the magnetic background is given by the inverse of $T \equiv K + M_0$. Before computing the inverse, we translate the spinor to the form $\psi_p = (c_{\uparrow p^+,m}, c_{\downarrow p^-,m})$, where $p^\pm = \mathbf{p} \pm \mathbf{Q}/2$ so that the matrix T is diagonal in momentum and frequency space. This implies that T is given by

$$T_{pq} = \delta_{pq} \begin{pmatrix} G^{-1}_{p^+,m} & \Delta \\ \Delta & G^{-1}_{p^-,m} \end{pmatrix}, \tag{2.6}$$

where $\Delta = US$ with μ_0 in the propagators replaced $\mu \equiv \mu + Un$. The off-diagonal contributions correspond to the spin-flip scattering processes induced by the magnetic configuration along the x and y spin axes. The uniform charge distribution simply redefines the chemical potential. The momentum translation of the fermions likewise affects the interaction matrices M and V. In the new fermion basis, the Gaussian fluctuations interact with the fermions via

$$M_{pq} = \begin{pmatrix} \rho_{p-q} + \phi^z_{p-q} & \phi^-_{p-q+Q} \\ \phi^+_{q-p+Q} & \rho_{p-q} - \phi^z_{p-q} \end{pmatrix}, \tag{2.7}$$

where the four-vector $Q = (\mathbf{Q}, 0)$. The electromagnetic vertices are similarly influenced and we find they acquire matrix form $V(A) \rightarrow W(A)$. $W(A)$ can be written by substituting for $\epsilon^{\alpha_1 \cdots \alpha_n}_{p/2+q/2}$ in Eq. (1.8) the diagonal matrix

$$\Sigma^{n\alpha_1 \cdots \alpha_n}_{pq} = \begin{pmatrix} \epsilon^{\alpha_1 \cdots \alpha_n}_{p^+/2+q^+/2} & 0 \\ 0 & \epsilon^{\alpha_1 \cdots \alpha_n}_{p^-/2+q^-/2} \end{pmatrix}. \tag{2.8}$$

Therefore, the vertex with one photon now reads $W^1_{pq}(A) = g\Sigma^{1\alpha}_{pq} A^\alpha_{p-q}$.

The matrix T can now be diagonalized in spin space $T \rightarrow T^D \equiv T$ by transforming the spinor $\chi_p = U_p \psi_p$, with

$$U_p = \begin{pmatrix} \cos\theta_p & \sin\theta_p \\ -\sin\theta_p & \cos\theta_p \end{pmatrix} \tag{2.9}$$

where $\tan 2\theta_p = 2US/(\epsilon_{p^-} - \epsilon_{p^+})$. The Jacobian in the fermion measure of the path integral is trivial[23] under the above unitary transformation and the fermions χ_p correspond to the upper and lower Mott-Hubbard bands with dispersions

$$E^\pm_p = g_p \pm \sqrt{h_p^2 + \Delta^2}, \tag{2.10}$$

where $2g_p = \epsilon_{p^-} + \epsilon_{p^+}$ and $2h_p = \epsilon_{p^-} - \epsilon_{p^+}$. In this new basis for the fermions, the electromagnetic interaction is now given by a rotation of the matrix Σ, $\lambda^{n\alpha_1 \cdots \alpha_n}_{pq} = U^\dagger_p \Sigma^{n\alpha_1 \cdots \alpha_n}_{pq} U_q$ making the one-photon vertex now $W^1_{pq} = g\lambda^{1\alpha}_{pq} A^\alpha_{p-q}$. The coherence factors U_p arise from the mean-field magnetic state just as they arise in the mean-field description of BCS superconductors.[24] The spin and charge fluctuation fields are now $D_{pq} = U^\dagger_p M_{pq} U_q$. Hence, the total fermion action equals $\chi^\dagger_p [T_{pq} + W_{pq}(A) + UD_{pq}]\chi_q$. The new propagator matrix is given by

$$T^{-1}_{pq} = \delta_{pq} \begin{pmatrix} G^-_p & 0 \\ 0 & G^+_p \end{pmatrix} \tag{2.11}$$

with $G^\pm_p = 1/[-iw_m + E^\pm_p - \mu]$.

The fermions χ_p can now be integrated out in the background uniform charge density and magnetic ground state to give for the effective action

$$\mathrm{Tr}\ln[T + W(A) + UD]$$

$$= \mathrm{Tr}\ln[T] - \sum_{n=1}^{\infty} \mathrm{Tr}\{-T^{-1}[W(A) + UD]\}^n/n. \tag{2.12}$$

The saddle-point condition[23,26] is that the linear terms in Φ^μ from the above cancel those from $\Phi^{\dagger\mu}\Phi^\mu$ after the mean-field decomposition. We determine the saddle-point conditions in the absence of $\mathbf{A}$ since this has been introduced only as a weak perturbation to perform linear response. The saddle-point equations therefore become $n = (1/L)\sum_{\mathbf{p}} \{f^+_p + f^-_p\}$ and

$$1 = (U/L)\sum_{\mathbf{p}} (f^-_p - f^+_p)/(E^+_p - E^-_p) \tag{2.13}$$

for the S order parameter where $f^\pm_p \equiv f(E^\pm_p - \mu)$. Terms of quadratic or higher order in the spin and charge fluctuations describe the collective modes associated with spin waves, multiparticle excitations, and the like.[16] These terms although higher order in $1/S$, contain essential corrections to all linear-response functions, particularly spin-correlation functions. We omit these corrections for now and concentrate instead on the saddle-point transport properties in the presence of symmetry breaking.

In addition to the two self-consistency conditions for n and S that we obtained for the magnetic saddle points, we can determine $\mathbf{Q}$ from requiring that the free energy be minimized. Neglecting all spin and charge fluctuations beyond linear order, we obtain for the thermodynamic potential

$$\Omega = ULn^2 + ULS^2 - (1/\beta)\mathrm{Tr}\ln[T] + (1/\beta)\sum_n \mathrm{Tr}[-T^{-1}W(A)]^n/n. \tag{2.14}$$

The third term can be simplified using the identity for the fermionic Matsubara sum $\sum_m \ln[-iw_m + x] = \ln[1 + \exp(-\beta x)]$ up to irrelevant c numbers, giving for the $\mathbf{A}$-independent thermodynamic potential

$$\Omega_0 = ULn^2 + ULS^2 - (1/\beta)\sum_{p,\alpha=\pm} \ln[1 + e^{-\beta(E^\alpha_p - \mu)}]. \tag{2.15}$$

From the particle constraint, we obtain the equation for μ given by

$$1-\delta=(1/L)\sum_{\mathbf{p}}\{f_p^+ + f_p^-\}, \tag{2.16}$$

making $2n = 1-\delta$. Therefore for fixed doping and U/t, n is independent of $\mathbf{Q}$ and S unlike μ. The free energy $F_0 = \Omega_0 + \mu_0\langle N\rangle$ is finally given by

$$F_0/L = US^2 + Un^2 + \mu(1-\delta) - (1/\beta L)\sum_{p,\alpha=\pm}\ln[1+e^{-\beta(E_p^\alpha-\mu)}]. \tag{2.17}$$

In the zero-temperature limit $\beta\to\infty$, the free energy must go to the ground-state energy since the entropy is zero and we find $F_0\to E_0$, where

$$E_0/L = US^2+U(1-\delta)^2/4+(1/L)\sum_{\mathbf{p}}\{E_p^+f_p^+ + E_p^-f_p^-\} \tag{2.18}$$

just as we found in the previous article.[15] The saddle-point results can be equivalently obtained from minimizing F_0 with respect to S or n. The second term in the free energy is the repulsive energy of the uniform electron gas and is canceled by the positive background by charge neutrality and is irrelevant for any saddle-point analysis of $\mathbf{Q}$ and S.

B. Phase diagrams

The nontrivial saddle-point constraint Eq. (2.13), the particle constraint for μ, and the condition

$$\partial F_0/\partial\mathbf{Q}=0 \tag{2.19}$$

at fixed doping U/t and temperature comprise the four coupled integral equations that determine the saddle point with lowest free energy for states with uniform charge and spin-rotational symmetry breaking. In Fig. 4 we plot the phase diagram of the 2D Hubbard model at $U/t=4$ by solving the above equations on a 500×500 mesh of the Brillouin zone. At half-filling, up to the magnetic transition temperature $T_M = 0.73t$, we find that antiferromagnetic moment formation is favored. However, at any nonzero dopings, spiral states are more stable at low temperatures. For low dopings $\delta<0.11$, a (1,1) spiral where $Q_x = Q_y \neq \pi$ is favored whereas for dopings $0.11<\delta<0.45$, a (1,0) spiral where Q_x or $Q_y=\pi$ is formed.[14,16] The paramagnetic metal to spin-density-wave (SDW) boundary can be determined from Eq. (2.13) by setting $S=0$ which then reduces to $1 = U\chi(\mathbf{Q},T_M)$ where the spin susceptibility is given by

$$\chi(\mathbf{Q},T)=(1/L)\sum_{\mathbf{p}}\frac{f(\epsilon_p-\mu)-f(\epsilon_{p+Q}-\mu)}{\epsilon_{p+Q}-\epsilon_p}. \tag{2.20}$$

This instability criterion corresponds to the random-phase approximation (RPA) for the Hubbard model.[19] Even in more sophisticated approximations,[27] the phase boundary extends to considerable finite doping. Our analysis here goes beyond this phase boundary since the coupled integral equations probe the nature of the SDW states below the transition temperature $T_M(\delta)$ for any doping. From the instability criterion Eq. (2.20), we note that when there is a symmetric density of states for dispersion ϵ_p, the critical temperature satisfies $T_M(\delta) = T_M(-\delta)$. Specifically, a similar symmetry relation should hold for the physical Nèel temperature T_N which separates the long-range antiferromagnetically ordered insulator from the fluctuation dominated paramagnetic insulator. Typically T_N is nearly an order of magnitude lower than T_M and occurs at an experimentally observed temperature whereas $T_M(\delta=0)$ occurs above the melting point of the entire solid. Furthermore, the particle-hole symmetry even in the presence of spiral magnetic states[16] ensures that the order parameters also satisfy $\mathbf{Q}(\delta)=\mathbf{Q}(-\delta)$ and $S(\delta)=S(-\delta)$, implying that *the phase diagrams of the hole and electron-doped systems are the same.* Note that $F_0(\delta)\neq F_0(-\delta)$ and $\mu(\delta)=-\mu(-\delta)$. When the temperature is increased in any of the spiral states, there is a smooth second-order transition to the antiferromagnetic states for $\delta<0.28$ or a first-order transition into the paramagnetic state for $0.28<\delta<0.45$.

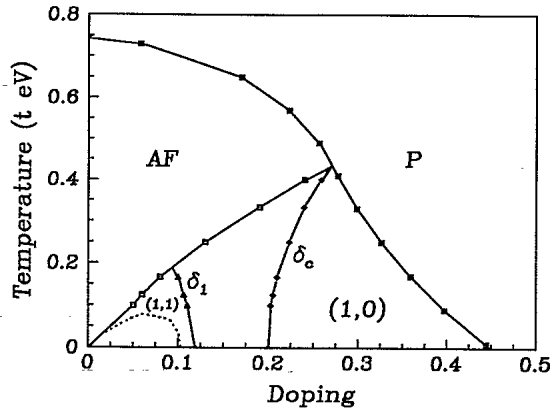

FIG. 4. The finite-temperature mean-field phase diagram of the 2D Hubbard model at $U/t=4$ displays paramagnetism (P), antiferromagnetism (AF), (1,1) spirals at low dopings and (1,0) spirals at moderate dopings. The Mott-Hubbard band crossing occurs at δ_c and the transition between the two types of spirals occurs at δ_1. R_H is positive in the region below the dotted curve and negative otherwise.

The bare parameters of the Hubbard model can be roughly approximated from various experimental measurements. Infrared measurements[28] fix the insulating gap of the antiferromagnetic samples to $\Delta\sim2$ eV. Neutron-scattering experiments on dynamical spin-spin correlations fix the spin-wave velocity[29] to $\hbar v_s = 0.85$ eV Å. Lastly, μSR measurements[30] give $\langle S\rangle\sim\frac{1}{3}$ for the spin-wave renormalized on-site magnetization. In the large U/t limit, the spin-wave velocity is proportional to $J=4t^2/U$, giving $J\sim0.16$ eV. Neglecting any self-energy corrections for the Mott-Hubbard band dispersions other than those that can be absorbed into S, the charge gap in the Mott-Hubbard picture is given by $\Delta = 2U\langle S\rangle$. Combining these results, we obtain $t\sim0.35$

eV and $U/t \sim 8$ for the 2:1:4 copper oxide in reasonable agreement with band-structure calculations.[31] This choice of t enables a direct fit of the bare Hubbard parameters to key experimental signatures without recourse to an *ad hoc* spin-renormalization factor necessary to obtain $t = 1$ eV.[16] Although the true values of J and Δ are significantly altered by spin-wave and other renormalization effects, the preceding analysis shows that the actual materials are most likely to be in the intermediate range of $U/t = 4$–12. Likewise, the exact positions of the paramagnetic-SDW boundary and other phase boundaries will be strongly influenced by fluctuation corrections since in a strictly 2D system, continuous symmetries cannot be broken. In fact, the observed Néel temperature T_N in the layered copper oxides is primarily determined by the spin-exchange constant in the c axis J_z. The coupling along the c axis and spin-wave fluctuations drives the Nèel temperature to what is experimentally observed $T_N \lesssim 0.1\ t$. We expect from Fig. 4, however, that the true phase diagram of the full three-dimensional (3D) system with fluctuations still contains a sizable region where spiral SDW states are stable.

Temperature and doping frustrate the order parameter S to zero as shown by the paramagnetic-SDW transition line in Fig. 4. Doping and temperature also frustrate the ground states by steadily moving $\mathbf{Q}$ away from $\mathbf{Q}_0$ and thus increasing the pitch $\mathbf{Q}_0 - \mathbf{Q}$. These combined effects move the upper and lower Mott-Hubbard bands closer together until they actually cross at doping δ_c shown in Fig. 4. This band crossing leads to a degeneracy of hole-like states in the top of the lower band with electronlike states at the bottom of the upper Mott-Hubbard band as shown in Fig. 5. Despite the indirect nature of the gap that connects the upper-band states to states near the chemical potential, their effects in optical absorption are nontrivial in the presence of spin waves, lattice excitations, and impurities. For dopings beyond δ_c, the effective Mott-Hubbard gap $\Delta_{\mathrm{MH}} \equiv \min(E_p^+) - \max(E_p^-) = 2US - 4t\cos(Q_x/2) - 4t\cos(Q_y/2) < 0$. The proximity of the upper Mott-Hubbard band and its role in the Hall coefficient and usual transport occurs at slightly higher dopings and temperature when $\Delta_1 = \min(E_p^+) - E_f \sim k_BT$. The temperature and doping dependence of the spiral order parameters $\mathbf{Q}$ and S, the presence of the upper Mott-Hubbard band, and the band crossing drastically alter transport behavior. To extract these quantities using linear response is nontrivial since in the Mott-Hubbard picture, the electromagnetic vertex has been completely modified for the spiral Mott-Hubbard bands.

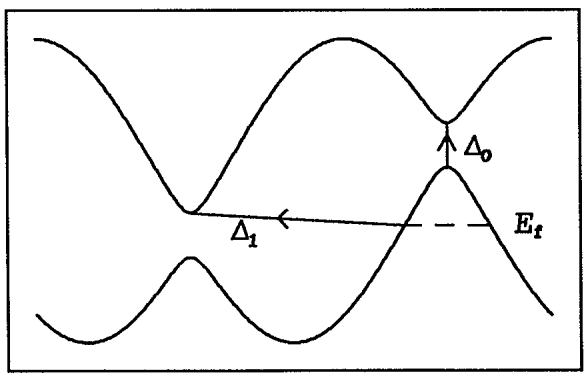

FIG. 5. The dispersions for the upper and lower Mott-Hubbard bands relative to the Fermi surface (E_F). The pockets of hole states at the top of the lower band and the pocket of electron states at the bottom of the upper band are related by an indirect optical gap (Δ_1) which is considerably lower than the minimum direct gap (Δ_0).

III. TRANSPORT FOR THE MOTT-HUBBARD SYSTEM

We now explore the role of the coherence factors U_p in linear-response functions at arbitrary temperature. The microscopic derivation provides a field-theoretic formalism for linear response in the presence of nontrivial ground states.[32]

The terms in the thermodynamic potential dependent on $\mathbf{A}$ give the effective action for the gauge fields coupled to the electrons moving in a ordered magnetic background. $\Omega(A)$ obtained in the last section in Eq. (2.14) is given by

$$\Omega(A) = (1/\beta)\sum_n \mathrm{Tr}[-T^{-1}W(A)]^n/n. \tag{3.1}$$

To obtain finite conductivities, we must again introduce a phenomenological lifetime for quasiparticle excitations in the upper and lower Mott-Hubbard bands by writing the propagators $G_p^{\pm} = 1/[-iw_m + E_p^{\pm} - \mu + i\,\mathrm{sgn}(w_m)\Gamma^{\pm}]$. The bandwidth of the lower Mott-Hubbard band varies from $4J$ for large U/t in the antiferromagnetic state to $8t$ for $\mathbf{Q} = 0$ in the ferromagnetic state. The spiral bandwidths are therefore in the range $4J < W < 8t$. Fits to the finite-frequency optical absorption in the normal state of the copper oxides[33,8] give $\Gamma(T) \sim 1 - 10\ k_BT$. This implies that in the region for small bandwidths and large quasiparticle widths, we have $\Gamma \sim W/3 \sim E_f/3$ using $T = 300$ K and $J = 0.16$ eV. In the other extreme of $W = 8t$ and $\Gamma = k_BT$, we find $\Gamma \sim E_f/100$ using $t = 0.35$. Therefore for some material parameters, the usual weak-scattering result $\Gamma \ll E_F$ is valid whereas for spirals with small pitch Γ can be a significant fraction of E_F. Since we are interested in the leading-order transport properties of the band-structure effects in the magnetic background, we assume for our calculation that the material properties allow us to safely assume $\Gamma < E_F$ and neglect any momentum dependence to Γ (Ref. 34) in addition to the vertex corrections that lead to the transport relaxation time.

A. Absence of paramagnetic currents

At finite doping, twisted antiferromagnetic order gives rise to pockets of holes at finite wave vectors. We verify that these pockets do not give rise to currents in the absence of an external field. From Eq. (1.13), we obtain that the response to zero order in the external fields is

$$\delta_0 \mathcal{J}_q^{\alpha} = (e/V\beta)\delta_{w_n,0}\delta_{\mathbf{q},0}\sum_p \{G_p^-[\lambda_{pp}^{1\alpha}]^{--} + G_p^+[\lambda_{pp}^{1\alpha}]^{++}\}, \tag{3.2}$$

where the superscripts on the vertex functions λ denote the matrix element, e.g., $[\lambda]^{-+} \equiv [\lambda]^{12}$. Since the band electrons are momentum eigenstates, the only contribution is from zero-momentum, zero-frequency photons. Using the definition of the matrices Σ and U, we find

$$\lambda_{pp}^{1\alpha} = \begin{pmatrix} E_p^{-\alpha} & F_p^{\alpha} \\ F_p^{\alpha} & E_p^{+\alpha} \end{pmatrix}, \tag{3.3}$$

where $F_p^{\alpha} = -\sin 2\theta_p \; h_p^{\alpha}$ and $E_p^{\pm\alpha} = \partial E_p^{\pm}/\partial p^{\alpha}$. Note that in the long-wavelength limit, the diagonal part of the single-photon vertex for the new band fermions is just given by the group velocities $E_p^{\pm\alpha}$ as in usual Fermi liquids. For a transition between bands or a finite momentum transfer, however, the vertex is nontrivial involving the angle θ_p. Evaluating the Matsubara sum, we find the crystal current in the absence of any fields to be

$$\delta_0 \mathcal{J}_q^{\alpha} = (e/V)\delta_{w_n,0}\delta_{\mathbf{q},0} \sum_{\mathbf{p}} \{E_p^{-\alpha} f_p^{-} + E_p^{+\alpha} f_p^{+}\}. \tag{3.4}$$

The group velocity can be written $E_p^{\pm\alpha} = g_p^{\alpha} \pm h_p^{\alpha} \cos 2\theta_p$. Under the translation plus inversion operation $\mathbf{p} \rightarrow -\mathbf{p} - \mathbf{Q}$, we note $g_p \rightarrow g_p$ and $h_p \rightarrow h_p$ giving $E_p^{\pm} \rightarrow E_p^{\pm}$. In contrast, since $g_p^{\alpha} \rightarrow -g_p^{\alpha}$ and $h_p^{\alpha} \rightarrow -h_p^{\alpha}$ the group velocities are odd under this transformation and hence $\delta_0 \mathcal{J}_q^{\alpha} = 0$. Despite the anisotropic Fermi surface for the states in the lower and upper Mott-Hubbard bands for spiral antiferromagnetism, there is no true crystal momentum reflecting the fact that the gaps for the original up- and down-spin electrons open on opposites sides of the initial Brilliouin zone.[16]

B. Ordinary conductivity

The usual conductivity is obtained from the pieces in the effective action quadratic in $\mathbf{A}$. These consist of one-loop graphs with two W^1 vertices and a graph with one W^2 vertex. The fermion lines in the loop graphs can be from the identical band or from different bands. In the latter type, the absorption and emission of a photon interchanges the band index from lower to upper or vice versa. In total, there are six diagrams that contribute to $\delta_1 \mathcal{J}_q^{\alpha}$ proportional to $\mathbf{a}^E$ and six proportional to $\mathbf{a}^B$. The imaginary part of the response from the interband diagrams is crucial for the cancellation of the diamagnetic graph with one W^2 vertex. From Eq. (3.3), we simplify the one-photon vertices and find the contribution of the six diagrams to linear order in the electric gauge potential to be

$$\delta_1 \mathcal{J}_q^{\alpha} = -a_n^{E\beta}(e^2/V\beta) \sum_{p,\mu=\pm} \left\{ E_p^{\mu\alpha} E_p^{\mu\beta} \sum_m G_{p,m}^{\mu} G_{p,m+n}^{\mu} - [\lambda_{pp}^{2\alpha\beta}]^{\mu\mu} \sum_m G_p^{\mu} \right\}, \tag{3.5}$$

$$-a_n^{E\beta}(e^2/V\beta) \sum_p \left\{ F_p^{\alpha} F_p^{\beta} \sum_m (G_{p,m}^{-} G_{p,m+n}^{+} + G_{p,m}^{+} G_{p,m+n}^{-}) \right\}. \tag{3.6}$$

The first two terms correspond to the four single-band pieces and the last two terms to the mixed-band pieces. To obtain finite dc conductivity the $w_n = 0$ contribution of the first and last two terms must cancel the entire second term for each band. From the definition of Σ and U, we find for the W^2 vertex,

$$\lambda_{pp}^{2\alpha\beta} = \begin{pmatrix} E_p^{-\alpha\beta} + C_p^{\alpha\beta} & H_p^{\alpha\beta} \\ H_p^{\alpha} & E_p^{+\alpha\beta} - C_p^{\alpha\beta} \end{pmatrix}. \tag{3.7}$$

Here, the coherence term $C_p^{\alpha\beta} = (\sin 2\theta_p/\Delta) F_p^{\alpha} F_p^{\beta}$ and the band-mixing term is $H_p^{\alpha\beta} = -\sin 2\theta_p \; F_p^{\alpha\beta}$ with $F_p^{\alpha\beta} = \partial F_p^{\alpha}/\partial p^{\beta}$. Unlike the one-photon vertex, the diagonal terms of the two-photon vertex is not simply $E_p^{\pm\alpha\beta}$ as in Fermi liquids but receives a correction of order $1/U$ from $C_p^{\alpha\beta}$. Expressing the first Matsubara sum in Eq. (3.5) at $w_n = 0$ as a partial derivative with respect to E_p^{μ} as in Sec. I, we see that it cancels with the $E_p^{\mu\alpha\beta}$ piece from the W^2 vertex. The $C_p^{\alpha\beta}$ term from the W^2 vertex cancels with the last two interband Matsubara sums at $w_n = 0$. To see this, we make the standard deformation in the complex plane[24] for the last two sums which gives

$$(1/\beta) \sum_m G_{p,m}^{-} G_{p,m}^{+} = (f_p^{+} - f_p^{-})/[E_p^{+} - E_p^{-}]. \tag{3.8}$$

The difference in the denominator is just the direct gap between the two bands and can be written $1/[E_p^{+} - E_p^{-}] = \sin 2\theta_p/2\Delta$ which when multiplied by the two factors of F is just the coherence term from the W^2 vertex. As in the case of the narrow-band metal, we find that the entire diamagnetic term is exactly canceled for any doping and temperature by the real part of the single- and mixed-band loop graphs. The cancellation of the diamagnetic term in the normal state required the interaction of the lower band with the upper band to cancel the order $1/U$ correction to the diamagnetic vertex even though the Fermi surface is entirely in the lower band at finite doping. It is apparent that the microscopic interactions of the bands which is beyond standard Bloch-Boltzmann theory was necessary to prove this cancellation.

The real part of the first term at $w_n \neq 0$ in Eq. (3.5) is exactly the standard result from Bloch-Boltzmann theory for electrical conductivity. Performing the Matsubara sums after introducing the retarded and advanced Green's functions and doing the analytic continuation for $\mathrm{sgn}(w_n) > 0$ as outlined in Sec. I, we find in the Fermi-liquid limit of $\Gamma < E_F$ that the imaginary part of the sum gives the usual term $\partial f_p^{\mu}/\partial E_p^{\mu}$ for $w \rightarrow 0$. For sufficiently low temperatures, i.e., when $k_B T \ll \Delta_1$, the lower band dominates the conductivity. Partially integrating in momentum space, the real part of the linear response to the $\mathbf{E}$ field is given by $\delta_1 \mathcal{J}_q^{\alpha} = \sigma_0^{\alpha\beta} E_w^{\beta}$, where

$$\sigma_0^{\alpha\beta} = (e^2\tau^-/V)\sum_{\mathbf{p}} E_p^{-\alpha\beta} f(E_p^- - \mu). \tag{3.9}$$

We recognize this is as the volume form of the Bloch-Boltzmann result which conventionally is written as a Fermi surface integral as in Eq. (1.20). At zero temperature for $\delta \to 0$, we can approximate $f(E_p^- - \mu) = 1$ making the integrand a total derivative and using periodic boundary conditions; we get $\sigma_0^{\alpha\beta} \to 0$ for the completely filled lower Mott-Hubbard band. It is clear that $\sigma_0^{xx} = \sigma_0^{yy}$ only for antiferromagnetism and $(1,1)$ spirals where $Q_x = Q_y$. In addition to the nonvanishing components σ_0^{xx} and σ_0^{yy} that one finds for the narrow-band metal with no symmetry-breaking order parameters, there is an additional anisotropic component σ_0^{xy} specific to (1,1) spirals. This off-diagonal conductivity can be brought to the form

$$\sigma_0^{xy} = (e^2\tau^-/V)\sum_{\mathbf{p}} (\sin^3 2\theta_p/\Delta) h_p^x h_p^y \, f(E_p^- - \mu). \tag{3.10}$$

For $(1,0)$ spirals and antiferromagnetism, $h_p^y = \sin p_y$ while the dispersion depends only on $\cos p_y$. Therefore the integrand is odd under the parity transformation $p_y \to -p_y$, making σ_0^{xy} vanish for $(1,0)$ spirals. In twinned single crystals, the signature of a $(1,0)$ spiral is the anisotropy $\sigma_0^{xx} \neq \sigma_0^{yy}$ whereas for the $(1,1)$ spiral, the unambiguous signature is the nonvanishing tensor σ_0^{xy}. Both of these anomalous coefficients vanish for paramagnetic, antiferromagnetic, and ferromagnetic states. We plot the conductivity tensor divided by the lifetime as a function of temperature at fixed doping in Fig. 6 for the self-consistent $(1,1)$ spiral at $U/t = 6$. Note that for the 2D tight-binding model, the momentum sums become $(1/V)\sum_{\mathbf{p}} \to (1/d)(1/2\pi)^2 \int d^2p$, where d is the unit cell spacing along the c axis and the momentum integral is to be performed over the 2D Brillioun zone. The temperature dependence of the conductivities is a convolution of $\Gamma^{\pm}(T) \equiv \Gamma(T)$ and the momentum integral for

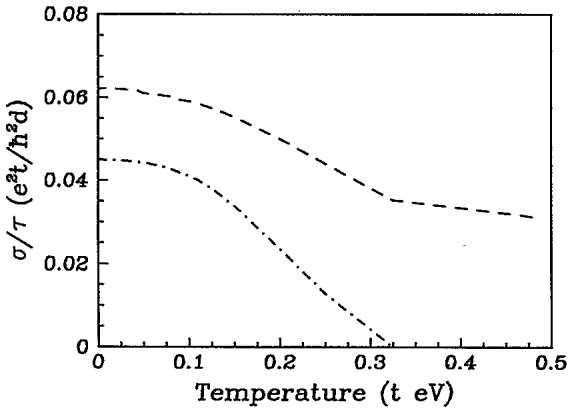

FIG. 6. The anisotropic conductivity σ_0^{xy}/τ (dotted-dashed line) is a significant fraction of the usual conductivity σ_0^{xx}/τ (dashed line) for $(1,1)$ spirals. Here, $U/t = 6, \delta = 0.1$ and the conductivities are in units of $e^2t/\hbar^2d$, where d is the lattice constant in the c direction.

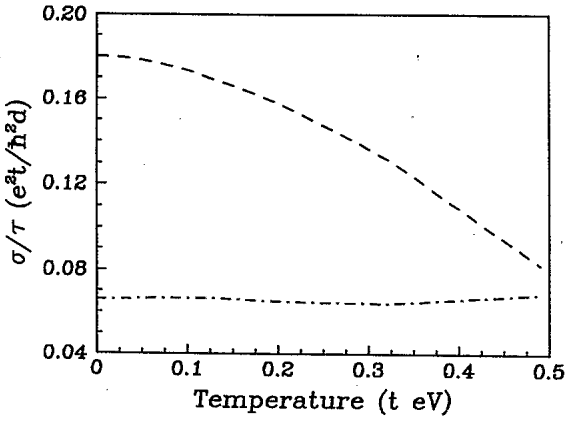

FIG. 7. The fall of σ_0^{xx}/τ (dashed line) with temperature for $(1,0)$ spirals reflects the evolution of the pitch with temperature whereas the conductivity σ_0^{yy}/τ remains constant. Here $U/t = 6$ and $\delta = 0.2$.

the conductivity. We obtain the residual temperature dependence from the Fermi-surface changes by considering $\sigma_0^{\alpha\beta}/\tau$. We note that the anisotropic component is a significant fraction of the usual conductivity and vanishes when $\mathbf{Q}$ unwinds to $\mathbf{Q}_0$. From the shape of the temperature curve, we can conclude the conductivities decrease more rapidly than τ. This is very unsatisfactory since the experimentally observed resistivity appears to be linear in temperature for moderate dopings. We must assume that quantities sensitive to the absolute value of τ like the conductivities require a better knowledge of the dynamical quasiparticle renormalizations and the concomitant vertex renormalizations in the spiral ground states. The two nonvanishing transport coefficients for $(1,0)$ spirals are plotted as a function of temperature in Fig. 7. The conductivity in the antiferromagnetic y direction σ_0^{yy} is always much smaller than the conductivity in the spiral direction σ_0^{xx} which is maximized when $\mathbf{Q} = (0,\pi)$, the column state.[16] The conductivity σ_0^{xx} decreases for increasing temperature until it coincides with σ_0^{yy} near the spiral-antiferromagnetic transition.

C. Hall conductivity

Terms cubic in $\mathbf{A}$ in the effective action $\Omega(A)$ give rise to the Hall conductivity. Among these terms, we concentrate on those that appear with one power of $\mathbf{a}^E$ and $\mathbf{a}^B$ in the induced current $\delta_2 \mathcal{J}_q^{\alpha}$. For diagrams with a single-band index, these diagrams are exactly those in Fig. 2. The diamagnetic term with one W^3 vertex is independent of $\mathbf{q}$ and w_n. As in the case of the tadpole diagram with one W^2 vertex considered above, it is canceled by the real part of the two triangle and three two-vertex graphs evaluated at zero momentum and zero frequency after including the interband terms. The second two-vertex graph is independent of $\mathbf{q}$ and is canceled by the trian-

gle graphs evaluated at $\mathbf{q} = 0$ after including interband processes. The third two-vertex graph is independent of w_n but has no pieces linear in $\mathbf{q}$. Since these calculations have no measurable consequences we leave this as a check for the reader. For the Hall conductivity, contributions to linear order in $\mathbf{q}$ and w_n come from the two triangle graphs and the first two-vertex graph in Fig. 2. These loop graphs with only the lower band included give

$$\delta_2 \mathcal{J}^{\alpha}_{\mathbf{q},w_n} = (e^3/V\beta) a^{E\beta}_{w_n} a^{B\gamma}_{q} \sum_{\mathrm{p}} \Big\{ -E^{-\alpha}_{p}(E^{-\gamma\beta}_{p} + C^{\gamma\beta}_{p}) \sum_{m} G^{-}_{p^-,m} G^{-}_{p^+,m+n} + E^{-\alpha}_{p} E^{-\gamma}_{p} [\lambda^{1\beta}_{p^+p^+}]^{--} \sum_{m} G^{-}_{p^-,m} G^{-}_{p^+,m} G^{-}_{p^+,m+n} + E^{-\alpha}_{p} E^{-\gamma}_{p} [\lambda^{1\beta}_{p^-p^-}]^{--} \sum_{m} G^{-}_{p^-,m} G^{-}_{p^+,m} G^{-}_{p^-,m-n} \Big\}. \tag{3.11}$$

Except for the appearance of the λ matrix in the triangle graphs and the coherence term $C^{\gamma\beta}_{p}$ in the two-vertex graph, this result is similar to the narrow band metal worked out in Sec. I. The terms linear in $\mathbf{q}$ from the Green's functions in the two triangle graphs cancel each other. Expanding the Green's functions in the two-vertex graph and the λ matrix, we find

$$\delta_2 \mathcal{J}^{\alpha}_{q} = (e^3/2V\beta) a^{E\beta}_{w_n} \Big[(q^{\delta} a^{B\gamma}_{q} - q^{\gamma} a^{B\delta}_{q}) \sum_{\mathrm{p}} E^{-\alpha}_{p} E^{-\gamma}_{p} E^{-\beta\delta}_{p} - (q^{\delta} a^{B\gamma}_{q}) \sum_{\mathrm{p}} E^{-\alpha}_{p} C^{\gamma\beta}_{p} E^{-\delta}_{p} \Big] \sum_{m} [G^{-}_{p,m}]^2 (G^{-}_{p,m+n} - G^{-}_{p,m-n}). \tag{3.12}$$

The first momentum sum has the usual gauge-invariant form whereas the second anomalous term depends on the coherence term from the W^2 vertex in the first two-vertex graph.

Like the diamagnetic term, the appearance of the coherence term in the Hall conductivity is canceled by including the interaction matrix element of the lower-band with the upper-band. To see this we consider the triangle graphs shown in Fig. 8 with two lower-band fermion lines and one upper-band fermion line. Evaluating the graphs in Fig. 8 using the diagrammatic rules, we obtain

$$\delta^{IB}_{2} \mathcal{J}^{\alpha}_{q} = (e^3/V\beta) a^{E\beta}_{w_n} a^{B\gamma}_{q} \sum_{\mathrm{p}} \Big\{ [\lambda^{1\alpha}_{p,p+q}]^{--} [\lambda^{1\beta}_{p,p}]^{+-} [\lambda^{1\gamma}_{p+q,p}]^{-+} \sum_{m} G^{+}_{p,m} G^{-}_{p+q,m} G^{-}_{p,m-n} + [\lambda^{1\alpha}_{p-q,p}]^{--} [\lambda^{1\beta}_{p,p}]^{-+} [\lambda^{1\gamma}_{p,p-q}]^{+-} \sum_{m} G^{+}_{p,m} G^{-}_{p-q,m} G^{-}_{p,m+n} \Big\}, \tag{3.13}$$

where we have chosen the loop momenta in order to simplify the upper-band Green's function. From the relation

$$[\lambda^{1\alpha}_{p+aq,p+bq}]^{\mu\mu} = E^{\mu\alpha}_{p} + \{(a+b)/2\} q^{\delta} E^{\mu\alpha\delta}_{p} + O(q^2), \tag{3.14}$$

we see that the pieces linear in $\mathbf{q}$ from the λ terms with index α cancel. The pieces linear in $\mathbf{q}$ from the off-diagonal λ components can be obtained using the general result

$$[\lambda^{1\gamma}_{p+aq,p+bq}]^{-+} = F^{\gamma}_{p} + q^{\delta}[(a+b) H^{\gamma\delta}_{p} + (\sin 2\theta_p/\Delta) F^{\delta}_{p} (b E^{-\gamma}_{p} - a E^{+\gamma}_{p})]/2, \tag{3.15}$$

$$[\lambda^{1\gamma}_{p+aq,p+bq}]^{+-} = F^{\gamma}_{p} + q^{\delta}[(a+b) H^{\gamma\delta}_{p} + (\sin 2\theta_p/\Delta) F^{\delta}_{p} (a E^{-\gamma}_{p} - b E^{+\gamma}_{p})]/2. \tag{3.16}$$

Inserting $a = 1, b = 0$ for the first diagram and $a = 0, b = -1$ for the second diagram, we find that the linear pieces in $\mathbf{q}$ again cancel leaving only the contribution from the Green's functions. If we introduce the retarded and advanced Green's functions to evaluate the Matsubara sum, we would find the integral in the complex plane is dominated by the quasiparticle poles in the lower band near the chemical potential at temperatures where $\Delta_1 \gg k_B T$. Hence we can replace the $i w_m$ in the upper-band Green's function by the pole at $E^{-}_{p} - \mu$, making $G^{+}_{p,m} = 1/[E^{+}_{p} - E^{-}_{p}] = \sin 2\theta_p/2\Delta$ as we showed by exact evaluation for the diamagnetic cancellation. Lastly, expanding the Green's functions, we get

$$\delta^{IB}_{2} \mathcal{J}^{\alpha}_{q} = (e^3/2V\beta) a^{E\beta}_{w_n} q^{\delta} a^{B\gamma}_{q} \sum_{\mathrm{p}} E^{-\alpha}_{p} E^{-\delta}_{p} (\sin 2\theta_p/\Delta) F^{\beta}_{p} F^{\gamma}_{p} \sum_{m} [G^{-}_{p,m}]^2 (G^{-}_{p,m+n} - G^{-}_{p,m-n}), \tag{3.17}$$

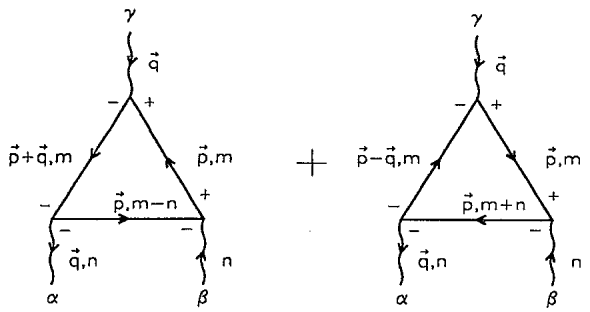

FIG. 8. The two triangle graphs involving interband processes which cancel the coherence terms in the Hall conductivity obtained from a single band alone.

which precisely cancels the $C_p^{\alpha\beta}$ term from Eq. (3.12). The Matsubara sum in the remaining term in Eq. (3.12) can be evaluated using standard techniques[18] giving finally for the Hall conductivity the canonical answer,

$$\sigma_H^{\alpha\beta\epsilon} = -\ (e^3\tau^-/V) \times \sum_{\mathbf{p}} E_p^{-\alpha}(\mathbf{E}_p^- \times \nabla)^\epsilon E_p^{-\beta}(-\partial f_p^-/\partial E_p^-), \tag{3.18}$$

where $\mathbf{E}_p^-$ denotes the group-velocity vector. The volume form of the Hall conductivity for a magnetic field along the c axis can be brought to the form

$$\sigma_H^{xyz} = -\ (e^3\tau/V) \times \sum_{\mathbf{p}} (E_p^{-xx}E_p^{-yy} - E_p^{-xy}E_p^{-yx}) f(E_p^- - \mu), \tag{3.19}$$

where we have used $\Gamma^\pm \equiv \Gamma$. At zero-temperature, the nontrivial coherence terms of order $1/U$ from the two-photon vertex are canceled by including interband interactions giving the conventional transport formula for the Hall conductivity. Therefore, response functions in the limit $q \to 0$ are entirely determined by the group velocity vectors. The fine structure of the band itself and the interactions of the upper and lower Mott-Hubbard bands are of importance only for quantities like the optical conductivity.

The cancellation of the coherence term in Eq. (3.12) is strictly valid only in the Fermi-liquid limit $\Gamma^\pm \ll E_F$ and in the low-temperature limit $k_BT \ll \Delta_1$. These assumptions allowed us to replace the upper-band Green's function by the quasiparticle pole at $E_p^- - \mu$. However, when $k_BT \sim \Delta_1$ and $\Delta_{\rm MH} \leq 0$, there is a degeneracy in the electronic spectrum between states in the upper and lower bands. In this regime when the occupation of the states in the bottom of the upper band is not suppressed, the dc transport can occur by scattering of lower- (upper-) band states to lower- (upper-) band states and lower- (upper-) band states to upper- (lower-) band states. This requires that we treat the Matsubara sum multiplying the $C_p^{\gamma\beta}$ term in Eq. (3.12) differently. We need to include the quasiparticle pole at $E_p^+ - \mu$ as well, which then gives rise to an unconventional contribution to the conductivity when $f(E_p^+ - \mu)$ is sizable. It is precisely in the interband transitions, where coherence terms arise, that corrections to the Bloch-Boltzmann analysis emerge. In contrast, the coherence term from the diamagnetic diagram is uninfluenced at finite temperature and is always canceled by the real part of the other diagrams to each order at zero external four momentum, i.e., at $q = 0$. For our analysis of the Hall coefficient, we present the results at temperatures where $k_BT < \Delta_1$ where interband effects can be ignored.

Since spirals create pockets of holes states,[16] the Hall coefficient has a $1/\delta$ dependence at low dopings which then dramatically goes to zero and changes sign, reflecting the significant changes in the Fermi surfaces at higher dopings. The Hall coefficient $R_H = \sigma^{xyz}/\sigma_0^{xx}\sigma_0^{yy}$ is manifestly independent of τ in the conventional Fermi-liquid limit $\Gamma \ll E_F$, where in addition the momentum dependence of the scattering time is neglected. From the particle-hole symmetry of spiral magnetic states, we find that the Hall coefficient of the electron- and hole-doped materials are related by $R_H(\delta) = -R_H(-\delta)$. In Fig. 9, we plot R_H for the commensurate antiferromagnetic state at three temperatures $\beta = 1000/t$, $20/t$, and $5/t$ with $\Delta = t$ fixed. The Hall coefficient is always negative at finite doping and diverges rapidly as we increase the temperature for moderate dopings. At the mean-field level, there are no pockets for the antiferromagnetic state which has dispersion $E_p^\pm = \pm\sqrt{\epsilon_p^2 + \Delta^2}$. Consequently, the Fermi surface at any finite doping encloses the origin and the point $\mathbf{Q}_0$. In the two-sublattice picture, the Fermi surface of the antiferromagnetic state encloses only the origin making a change in sign of R_H impossible. In contrast, a doubling of the Brillioiun zone becomes necessary for incommensurate magnetic states. Near $\delta \sim 1$, where the dispersion is almost parabolic, the temperature dependence disappears for the antiferromagnetic state. A major reason for the sensitivity of R_H to temperature

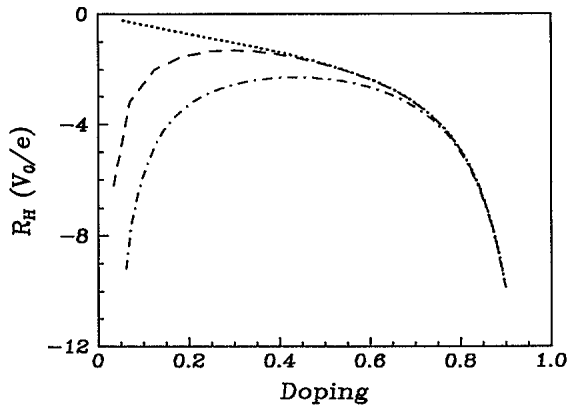

FIG. 9. The Hall resistivity in units of V_0/e where V_0 is the volume of the unit cell for the antiferromagnetic state when $\Delta = t$ vs doping for $\beta = 1000/t, 20/t$, and $5/t$, shown as a dotted line, dashed line, and dotted-dashed line, respectively. At mean field, R_H is always negative and exhibits a strong temperature dependence at low doping due to nonparabolic effects.

near moderate doping is the vicinity of the singularity in the density of states at the upper edge of the lower Mott-Hubbard band when $\mathbf{Q} = \mathbf{Q}_0$.

Whereas commensurate antiferromagnetism predicts $R_H(\delta) < 0$ for any $\delta > 0$, spiral states always lead to a sign change at the mean-field level. In Fig. 10 we plot the Hall coefficient for a $(1,1)$ spiral with $Q = 5\pi/6$ and a $(1,0)$ spiral with $Q_x = 3\pi/4$, $Q_y = \pi$, and ferromagnetism all at $\Delta = t$ and zero temperature. We note that at small doping $R_H \sim 1/\delta$ while at intermediate doping, there is always a change in sign in the range $0 < \delta < \frac{1}{2}$ whenever $\pi > Q > 0$. R_H for the ferromagnetic state with dispersion $\epsilon_p \pm \Delta$ at doping δ is the same as the R_H of the paramagnetic state with doping $2\delta - 1$ and therefore has a sign change exactly at quarter filling. We note that the slope discontinuities in R_H for the spiral states is due to logarithmic singularities in the densities of state in the Mott-Hubbard bands.[16] For very high doping $\delta \sim 1$, the curves in Fig. 10 converge since the dispersion is nearly parabolic for any $\mathbf{Q}$ and S. Unlike the pockets that may arise for the antiferromagnetic state when self-energy corrections are performed, the pockets for the spiral states are very robust and extend to significant doping for any intermediate value of U/t. We combine the doping dependence of S and Q for the spiral states at zero temperature and plot R_H in units of V_0/e where V_0 is the unit cell volume for $U/t = 4, 5, 6, 7.5$ in Fig. 11. For the 2:1:4 copper oxide with a unit cell of 94.2 Å^3, this becomes $V_0/e = 5.89 \times 10^{-4}$ cm^3/Coulomb. The discontinuities in R_H reflect the transition from $(1,1)$ spirals to $(1,0)$ spirals. Near the sign change R_H drops precipitously and the Hall coefficient beyond the sign change is shown in dashed lines. In Fig. 12 we compare the dopings where a sign change occurs in each type of spiral with the doping where the transition between the two types of spirals occurs for $U/t \leq 10$. For $U/t < 6$, the sign change occurs in the $(1,1)$ spiral states whereas for $U/t \geq 6$, the sign change occurs within the $(1,0)$ spiral states. For $7 < U/t < 12$, the sign change occurs when the $(1,0)$ spiral unwinds to the column state given by $\mathbf{Q} = (0,\pi)$ at

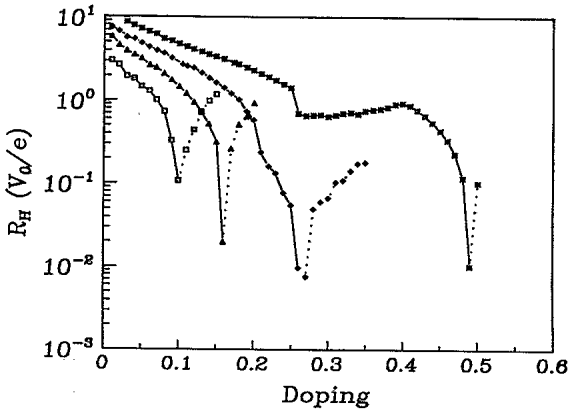

FIG. 11. The Hall resistivity for the 2D Hubbard model at $U/t = 4, 5, 6, 7.5$ (square, triangle, diamond, star) vs doping at zero temperature. Near half-filling $R_H > 0$ and the transition from $(1,1)$ to $(1,0)$ spirals does not interrupt the precipitous fall of R_H. The values of $-R_H$ beyond the sign change at δ_H are traced.

$\delta = \frac{1}{4}$. When $U/t > 12$, the $(1,1)$ spiral unwinds into the ferromagnetic state where the sign change then occurs at $\delta = \frac{1}{4}$ without any transition to the $(1,1)$ spiral. We note that when $U/t \leq 6$, most of the $(1,1)$ phase has a positive Hall coefficient and at higher dopings, the $(1,0)$ phase has a negative R_H. As we increase U/t, both phases have positive Hall coefficients until quarter filling. Ordinary antiferromagnetic ordering is inconsistent with the experimentally observed positive Hall coefficient at moderate doping whereas for spirals, the sign change can occur at any doping up to quarter filling. We can associate the doping-induced sign change of the Hall coefficient with the Fermi-surface topology change from pocket-type to one enclosing the origin which occurs at one of the saddle points[16] of E_p^-. The sign change occurs when $\mu \sim E_p^-$ and $\mathbf{p} = (-Q_x, \pi - Q_y/2)$, one of the saddle points for any S. Low-temperature data[35] on both the electron and hole copper oxides have always shown an anomalous reduction of R_H from $1/\delta$ at $\delta > 0.03$ along with a pre-

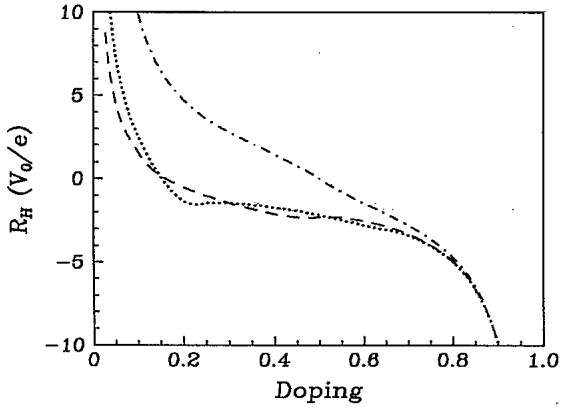

FIG. 10. The Hall resistivity for $(1,1)$ spiral (dotted line), $(1,0)$ spiral (dashed line), and the ferromagnetic state (dotted-dashed line) with $\Delta = t$ fixed. A sign change always occurs between $0 < \delta \leq 0.5$.

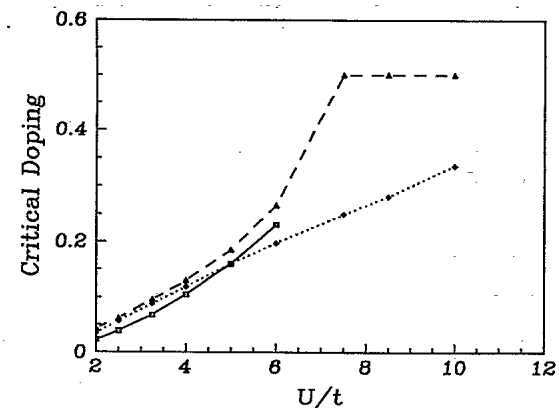

FIG. 12. The critical doping δ_H where R_H changes sign from being holelike to electronlike vs U/t for $(1,1)$ spirals (square) and $(1,0)$ spirals (triangle) at zero temperature. The $(1,1)$ to $(1,0)$ transition is labeled by the dotted curve.

cipitous fall and change in sign at $\delta \sim 0.1 - 0.2$. In our mean-field picture, this is consistent with $U/t = 4 - 6$ in remarkable agreement with the spin and optical data at half-filling.

Changes of the Fermi-surface topology with temperature also lead to a strong temperature dependence for R_H. The temperature dependence in Fig. 9 was entirely from nonparabolic effects since we kept Δ and $\mathbf{Q}$ fixed. Since the $(1,1)$ spiral phase has positive R_H and antiferromagnetism has negative R_H and considering the phase transition that occurs between the two at finite temperature as shown in Fig. 4, we expect a strong temperature dependence for R_H. The temperature T_H at which the sign change occurs increases with doping at first and then decreases to zero as shown by the dotted line in Fig. 4. Since the Hall-coefficient anomalies are associated with low-energy Fermi-surface-topology effects, we expect that the true temperature scale on which these effects occur will be lowered by spin-wave renormalization effects. These renormalizations change the magnetic order on a sufficiently short time scale to affect dynamics near the Fermi surface and possibly bring these transport anomalies into the observable temperature scale $T_N(\delta)$ rather than $T_M(\delta)$. Anomalous temperature dependences have been repeatedly observed in single-crystal data[12,36] where in the superconducting window, a strong temperature dependence is observed which is suppressed at both higher and lower dopings. From Fig. 13 we see the Hall number per unit cell $n_H = 1/R_H$ is flat at very low temperatures and then crosses over to a parabolic temperature dependence in the vicinity of the spiral-antiferromagnet transition. Experiments have focused on the temperature dependence below the sign change in the hole doped superconductors where a linear T dependence has been observed. In most of the copper-oxide samples the Hall number is found to increase with temperature in accordance with our mean-field results. We ascribe the unusual doping dependences observed in n_H for the copper oxides at moderate dopings to the Fermi-surface topology changes that induce a sign change in R_H naturally in the incommensurate SDW mean-field states of the 2D Hubbard model. If spin-wave effects in fact reduce the relevant temperature scales, these same effects may also account for the unusual temperature dependence of n_H.

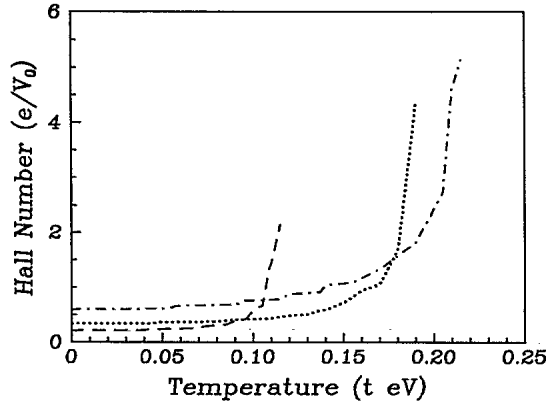

FIG. 13. The Hall number per unit cell $n_H = 1/R_H$ in units of e/V_0 vs temperature for the $(1,1)$ spiral at $U/t = 5$ and $\delta = 0.05, 0.10, 0.15$ shown as dashed, dotted, and dotted-dashed lines, respectively. Near the spiral-antiferromagnetic transition, the sign change in R_H leads to a strong temperature dependence for $n_H \sim 1/(T - T_H)$, where T_H is the temperature at which the sign change in R_H occurs.

In addition to the temperature dependence from the Fermi-surface changes, there is also an anomalous contribution related to the proximity of the upper band. When $\Delta_1 \sim k_B T$, the occupation of the upper-band states contributes to the conductivities. Although this requires a complete treatment of the loop graphs with both band electrons present as we mentioned earlier, a simpler approximation can be made by just adding the upper- and lower-band contributions separately. In this approximation, the Hall coefficient becomes

$$R_H = \frac{\sigma_{H-}^{xyz} + \sigma_{H+}^{xyz}}{(\sigma_{0-}^{xx} + \sigma_{0+}^{xx})(\sigma_{0-}^{yy} + \sigma_{0+}^{yy})}, \tag{3.20}$$

where the $\pm$ signs refer to upper and lower bands, respectively. This two-band formula explicitly avoids the band interactions which we know are nonvanishing from the microscopic calculation. For most U/t and $\delta > 0$, the region where $\Delta_1 \sim k_B T$ is where R_H is already negative, i.e., near the paramagnetic-SDW boundary. Since the sign of R_H is different for each band, the upper-band contribution in the above formula leads to a precipitous rise in R_H towards the paramagnetic value at the same doping and temperature. Unlike other two-band explanations for the temperature dependence R_H, the second band in this case arises naturally from the Hubbard model itself. The temperature dependence that arises from the upper band, however, is only important at relatively high temperatures near $T_M(\delta)$ and the low-temperature effects are entirely due to the lower Mott-Hubbard band.

At very low dopings $\delta < 0.03$, both the in-plane and out-of-plane resistivities diverge in the zero-temperature limit revealing an insulating behavior[33] contrary to the picture of a spiral metal presented here. However, in the moderate doping region, the materials are metallic at all temperatures and in some small window become superconducting. The mobility in the magnetic ground states of the 2D Hubbard model is influenced by the anisotropic topology of the hole pocket, the presence of nonlinear dispersive spin-wave modes, massive charge-fluctuation modes corresponding to interband transitions, and nontrivial distributions of the density of states near the Fermi level.[16] Although the spiral metal will in turn receive enormous corrections at small dopings, these fluctuations are suppressed energetically by an energy scale proportional to the inverse correlation length when long-range magnetic order is destroyed by frustration effects at moderate dopings. Interestingly, the destruction of the long-range order can be brought about precisely by the intrinsic degeneracies of the spiral states themselves.[16] In the presence of these domains, the Fermi surface becomes symmetric although still pocketlike and the short-ranged spiral may remain a metal to low temperatures.

Extensive neutron-scattering studies reveal that long-

range magnetic ordering is destroyed for $\delta > 0.03$ in the layered copper oxides.[37] At moderate doping, the correlation length is roughly the order of the interhole spacing. However, the spin-spin correlations are unlike a completely disordered state and strong fluctuations near $\mathbf{Q}_0$ are borne out by the nuclear relaxation measurements.[38] Due to the underlying lattice symmetry, a $(1,1)$ and $(1,0)$ spiral state with wave vector $\mathbf{Q}$ is energetically degenerate with four other states, respectively, in an oriented lattice. The equivalent states for a $(1,1)$ spiral are $Q^* = (Q_x, Q_y), (Q_x, -Q_y)$ and their reflections across the origin. For the $(1,0)$ spiral, they are $Q^* = (Q, \pi), (-Q, \pi)$ and their reflections across the line $Q_x = Q_y$. In the presence of an external electric field along the x axis, each of these states are distinguishable. A possible reconciliation of the NMR data with the neutron data is that moderate doping favors the creation of domains with the magnitude of the pitch fixed by the doping but the orientation varying among the degenerate states. Evidence for strong incommensurate fluctuations in the moderate doping region also comes from the prediction of a slightly non-Korringa relaxation rate for the oxygens and a strongly non-Korringa relaxation rate for the coppers.[39] Incommensurate order is also consistent with an increasing rms deviation of the local orienting field with doping observed in μSR relaxation measurements.[40] Lastly, anomalous double peaks in neutron scattering[37] for the 2:1:4 system could also be related to spiral states.

Most of the transport results we have calculated are exactly the same in the short-ranged domain structure. We consider the usual conductivity tensor evaluated for Q^*. In the integral in Eq. (3.9), if we replace $p_x \rightarrow -p_x$, we find that $\sigma_0^{\alpha\beta}(Q^*) = \sigma_0^{\alpha\beta}(Q)$ as long as $\alpha = \beta$. In contrast, the anisotropic component satisfies $\sigma_0^{xy}(Q^*) = -\sigma_0^{xy}(Q)$. Unlike the other components, the anisotropic element for $(1,1)$ spirals is canceled in samples with short-range order or crystals that are unoriented. Even though the Fermi surfaces of the degenerate spirals are on opposite sides, the diagonal components of the conductivity in the domain-averaged sample is the same as in the long-range ordered spiral metal. Inserting the same transformation in the integral for the volume form of the Hall conductivity in Eq. (3.19), we find that $\sigma_H^{xyz}(Q^*) = \sigma_H^{xyz}(Q)$ for both $(1,1)$ and $(1,0)$ spirals. The topology of the Fermi surface is the same for Q and Q^* and hence this result is not surprising. Bringing this all together, we find that since the Hall coefficient for the two degenerate spirals, it is unaffected by short-ranged ordering. The unusual temperature and doping dependence of the Hall coefficient is insensitive to the transition to short-ranged ordering which may itself be brought about by the lattice degeneracies of the spiral magnetic states.

IV. CONCLUSIONS

We have shown how the 2D Hubbard model away from half-filling involves a Mott-Hubbard band structure that recaptures the sign changes of the Hall coefficient with doping. These same Fermi-surface changes lead to a nontrivial temperature dependence for the Hall coefficient with sign changes at low doping. Spiral magnetic states, dynamically short ranged or long ranged, are rich enough to capture these anomalous sign changes. We have also shown that for a narrow-band system, residual temperature dependences in the transport coefficients can arise from an unconventional quasiparticle damping rate. However, the Fermi-liquid assumption combined with the pitch variations with temperature do not account for the linear resistivity. Obviously, the fluctuation corrections for the quasiparticle lifetimes of the spiral Mott-Hubbard bands is desirable. These corrections may lead to qualitative modifications in the short-ranged spiral where dynamical restoration of the broken symmetry takes place. It is not clear whether a long-wavelength spin-wave approximation described by the nonlinear σ model is sufficient to describe this restoration or whether short-wavelength topological excitations which probe the full Mott-Hubbard gap are necessary. In general, fluctuation corrections to the effective action $\Omega(A)$ will be of three types. The first consists of self-energy renormalizations to the fermion lines giving corrections to $\Gamma(\mathbf{p}, \epsilon)$. The second consists of electromagnetic vertex renormalizations which bring interband processes as corrections and most importantly modify the time scales involved in conductivity from the quasiparticle lifetime to the transport relaxation time. The third consists of diagrams where each photon is connected to a different loop and the loops are interconnected by fluctuations. In this latter type, the dispersion and renormalizations for the spin waves and their damping rate will provide important corrections to conductivity. Since such diagrams are higher order in $1/S$, they play an important role especially at moderate doping where the frustration of S is significant. These spin-wave renormalizations must play a crucial role in lowering the temperature scale on which anomalies in low-energy dynamical response occur. The mean-field predictions for R_H in the spiral magnetic states are indicative that further many-body corrections should be pursued completely, both from the standpoint of quantitative modifications of temperature scales as well as qualitative effects needed to explain the marginal Fermi-liquid behavior and high-temperature superconductivity.

ACKNOWLEDGMENTS

This work was supported in part by the Natural Sciences and Engineering Research Council of Canada.

[1] P. W. Anderson, Science **235**, 1196 (1987).
[2] N. F. Mott, Phys. Soc. London Sect. A **62**, 416 (1949); Rev. Mod. Phys. **40**, 677 (1968).
[3] H. J. Schulz, Phys. Rev. Lett. **64**, 1445 (1990); J.R. Schrieffer, X. G. Wen, and S. C. Zhang, Phys. Rev. B **39**, 11 663 (1989).
[4] P. W. Anderson, Phys. Rev. Lett. **65**, 2306 (1990); J. Engelbrecht and M. Randeria, *ibid.* **65**, 1032 (1990); M. Fabrizio, A. Parola, and E. Tosatti, Phys. Rev. B **43**, 1033 (1991).
[5] A. Moreo *et al.*, Phys. Rev. B **41**, 2313 (1990); A. Moreo

and D. J. Scalapino, *ibid.* **43**, 8211 (1991).
[6]P. W. Anderson, Phys. Rev. Lett. **64**, 1839 (1990); C. M. Varma, P.B. Littlewood, S. Schmitt-Rink, E. Abrahams, and A. Ruckenstein, *ibid.* **64**, 497 (1990); A. Virosztek and J. Ruvalds, Phys. Rev. B **42**, 4064 (1990).
[7]C.J. Olson *et al.*, Science **245**, 731 (1989).
[8]Z. Schlesinger *et al.*, Phys. Rev. Lett. **65**, 801 (1990); J. Orenstein *et al.*, Phys. Rev. B **42**, 6342 (1990); K. Kamaras *et al.*, Phys. Rev. Lett. **64**, 84 (1990).
[9]S. M. Hayden, Phys. Rev. Lett. **66**, 821 (1991).
[10]S. Martin *et al.*, Phys. Rev. Lett. **60**, 2194 (1988).
[11]T. Penney *et al.*, Phys. Rev. B **38**, 2918 (1988).
[12]T.R. Chien *et al.*, Phys. Rev. B **43**, 6242 (1991).
[13]B. I. Shraiman and E. D. Siggia, Phys. Rev. Lett. **62**, 1564 (1989); C. L. Kane *et al.*, Phys. Rev. B **41**, 2653 (1990).
[14]S. Sarkar, C. Jayaprakash, H. R. Krishnamurthy, and W. Wenzel, Phys. Rev. B **43**, 8775 (1991).
[15]S. John, P. Voruganti, and W. Goff, Phys. Rev. B **43**, 10 815 (1991).
[16]S. John and P. Voruganti, Phys. Rev. B **43**, 13 365 (1991).
[17]S. Trugman, Phys. Rev. Lett. **65**, 500 (1990); J. Ruvalds and A. Virosztek, Phys. Rev. B **42**, 399 (1990); J.H. Kim, K. Levin, and A. Auerbach, *ibid.* **39**, 11 633 (1989).
[18]A. Abrikosov, L. P. Gorkov, and I. E. Dzyaloshinskii, *Methods of Quantum Field Theory in Statistical Physics* (Prentice-Hall, Englewood Cliffs, NJ, 1963).
[19]S. Doniach and E. H. Sondheimer, *Green's Functions for Solid State Physicists* (Benjamin, Reading, 1974).
[20]K. G. Wilson, Phys. Rev. D **10**, 2445 (1974).
[21]B. Sakita, *Quantum Theory of Many-Variable Systems and Fields* (World Scientific, Singapore, 1985).
[22]D. Pines and P. Nozières, *The Theory of Quantum Liquids; Normal Fermi Liquids* (Benjamin, Reading, 1989).
[23]P. Ramond, *Field Theory: A Modern Primer* (Benjamin, Reading, 1981).
[24]A. Fetter and J. D. Walecka, *Quantum Theory of Many Particle Systems* (McGraw-Hill, New York, 1971).
[25]J. R. Schrieffer, *Theory of Superconductivity* (Benjamin, New York, 1964); G. D. Mahan, *Many Particle Physics* (Plenum, New York, 1981).
[26]E. Fradkin, *Field Theories of Condensed Matter Systems* (Addison-Wesley, Redwood City, 1991), p. 39.
[27]N. E. Bickers, D. J. Scalapino, and S. R. White, Phys. Rev. Lett. **62**, 961 (1989).
[28]Y. Tokura *et al.*, Physica C **162-164**, 1231 (1989).
[29]G. Aeppli *et al.*, Phys. Rev. Lett. **62**, 2052 (1989).
[30]A. Weidinger *et al.*, Phys. Rev. Lett. **62**, 102 (1989).
[31]L.F. Mattheiss, Phys. Rev. Lett. **58**, 1035 (1987).
[32]L.B. Ioffe and A.I. Larkin, Phys. Rev. B **39**, 8988 (1989).
[33]B. Batlogg, *High Temperature Superconductivity—Los Alamos Proceedings*, edited by K.S. Bedell *et al.* (Addison-Wesley, Redwood City, 1990).
[34]N.P. Ong, *Physical Properties of High-Temperature Superconductors*, edited by D.M. Ginsberg (World Scientific, Singapore, 1990), Vol. 2, p. 459.
[35]Z. Z. Wang, T. R. Chien, N.P. Ong, J. M. Tarascon, and E. Wang, Phys. Rev. B **43**, 3020 (1991); H. Takagi, S. Uchida, and Y. Tokura, Phys. Rev. Lett. **62**, 1197 (1989); N. P. Ong, Z. Z. Wang, J. Clayhold, J. M. Tarascon, L. H. Greene, and W. R. McKinnon, Phys. Rev. B **35**, 8807 (1987).
[36]M. Suzuki, Phys. Rev. B **39**, 2312 (1989); H. Takagi *et al.*, *ibid.* **40**, 2254 (1989).
[37]R.J. Birgeneau *et al.*, Phys. Rev. B **38**, 6614 (1988); **39**, 2868 (1989); J. M. Tranquada *et al.*, *ibid.* **38**, 2477 (1988).
[38]A. J. Millis, H. Monien, and David Pines, Phys. Rev. B **42**, 167 (1990); C. H. Pennington and C. P. Slichter, Phys. Rev. Lett. **66**, 381 (1991); R. E. Walstedt and W. W. Warren, Jr., Science **248**, 1082 (1990).
[39]N. Bulut, D. Hone, D. J. Scalapino, and N. E. Bickers, Phys. Rev. Lett. **64**, 2723 (1990).
[40]R. F. Kiefl *et al.*, Phys. Rev. Lett. **63**, 2136 (1989).